A systematic re-examination of processing of MHCI-bound antigenic peptide precursors by endoplasmic reticulum aminopeptidase 1

Received for publication, February 9, 2020, and in revised form, March 9, 2020 Published, Papers in Press, March 17, 2020, DOI 10.1074/jbc.RA120.012976

George Mavridis[‡], Richa Arya[§], Alexander Domnick[¶], Jerome Zoidakis[‖], Manousos Makridakis[‖], Antonia Vlahou[‖], Anastasia Mpakali[‡], Angelos Lelis[**], Dimitris Georgiadis[**], Robert Tampé[¶], Athanasios Papakyriakou[‡], Lawrence J. Stern[§], and Efstratios Stratikos[‡1]

*From the [‡]National Centre for Scientific Research Demokritos, Agia Paraskevi 15341, Greece, the [§]University of Massachusetts Medical School, Worcester, Massachusetts 01655, the [¶]Institute of Biochemistry, Biocenter, Goethe University Frankfurt, Max-von-Laue-Strasse 9, D-60438 Frankfurt/Main, Germany, the [‖]Centre of Basic Research, Biomedical Research Foundation of the Academy of Athens, Athens 11527, Greece, and the **Laboratory of Organic Chemistry, Chemistry Department, University of Athens, Athens 15772, Greece*

Edited by Peter Cresswell

Endoplasmic reticulum aminopeptidase 1 (ERAP1) trims antigenic peptide precursors to generate mature antigenic peptides for presentation by major histocompatibility complex class I (MHCI) molecules and regulates adaptive immune responses. ERAP1 has been proposed to trim peptide precursors both in solution and in preformed MHCI-peptide complexes, but which mode is more relevant to its biological function remains controversial. Here, we compared ERAP1-mediated trimming of antigenic peptide precursors in solution or when bound to three MHCI alleles, HLA-B*58, HLA-B*08, and HLA-A*02. For all MHCI-peptide combinations, peptide binding onto MHCI protected against ERAP1-mediated trimming. In only a single MHCI-peptide combination, trimming of an HLA-B*08-bound 12-mer progressed at a considerable rate, albeit still slower than in solution. Results from thermodynamic, kinetic, and computational analyses suggested that this 12-mer is highly labile and that apparent on-MHC trimming rates are always slower than that of MHCI-peptide dissociation. Both ERAP2 and leucine aminopeptidase, an enzyme unrelated to antigen processing, could trim this labile peptide from preformed MHCI complexes as efficiently as ERAP1. A pseudopeptide analogue with high affinity for both HLA-B*08 and the ERAP1 active site could not promote the formation of a ternary ERAP1/MHCI/peptide complex. Similarly, no interactions between ERAP1 and purified peptide-loading complex were detected in the absence or presence of a pseudopeptide trap. We conclude that MHCI binding protects peptides from ERAP1 degradation and that trimming in solution along with the dynamic nature of peptide binding to MHCI are sufficient to explain ERAP1 processing of antigenic peptide precursors.

Cytotoxic T-lymphocytes recognize infected or otherwise aberrant cells through specialized receptors that interact with ligands on the surface of somatic cells. The T-cell receptor can interact with the major histocompatibility complex class I molecules (MHCI)[2] that are located on the cell surface of all somatic cells and carry bound small peptides, called antigenic peptides (1). These peptides are generated intracellularly from the proteolytic degradation of antigenic proteins. During the latter parts of this pathway, N-terminally extended precursors of antigenic peptides are trimmed by ER-resident aminopeptidases ERAP1 and ERAP2 (2). Since its initial discovery, ERAP1 has emerged as an important component of the antigenic peptide generation pathway (3, 4). Accordingly, ERAP1 activity can influence the peptide cargo of MHCI and regulate the immunogenicity of cells, as demonstrated by several genetic knock-

This research was financed by the project "National Centre for Scientific Research Demokritos–Institute of Nuclear and Radiological Sciences and Technology, Energy, and Safety Research Activities in the Framework of the National RIS3" (MIS 5002559), implemented under the "Action for the Strategic Development on the Research and Technological Sector" program, funded by the Operational Program "Competitiveness, Entrepreneurship and Innovation" (Grant NSRF 2014–2020) and co-financed by Greece and the European Union (European Regional Development Fund). This work was also supported by the General Secretariat for Research and Technology and the Hellenic Foundation for Research and Innovation Postdoctoral Grant 303 (to A. M. and A. P.); a grant from the Harry J. Lloyd Charitable Trust (to E. S.); National Institutes of Health Grant AI038996 (to L. J. S.); a Reinhart Koselleck Project of the German Research Foundation (Deutsche Forschungsgemeinschaft) (to R. T.); ERC Advanced Grant 789121 (to R. T.); the Hellenic Foundation for Research and Innovation (HFRI) under the HFRI Ph. D. Fellowship Grant (Fellowship 157) (to G. M.); and State Scholarships Foundation Grant 2018-050-0502-15254 (to A. L.). The authors declare that they have no conflicts of interest with the contents of this article. The content is solely the responsibility of the authors and does not necessarily represent the official views of the National Institutes of Health.

This article was selected as one of our Editors' Picks.

This article contains Tables S1 and S2 and Figs. S1–S18.

[1] To whom correspondence should be addressed: National Centre for Scientific Research Demokritos, Patriarhou Gregoriou and Neapoleos 27, Agia Paraskevi, Athens 15341, Greece. E-mail: stratos@rrp.demokritos.gr or stratikos@gmail.com.

[2] The abbreviations used are: MHCI, major histocompatibility complex class I molecule(s); ERAP1, endoplasmic reticulum aminopeptidase 1; ERAP2, endoplasmic reticulum aminopeptidase 2; LAP, leucine aminopeptidase; DSF, differential scanning fluorimetry assay; RMSD, root mean square deviation; HLA, human leukocyte antigen; PLC, peptide-loading complex; SEC, size-exclusion chromatography; PDB, Protein Data Bank; MD, molecular dynamics; RMSF, root mean square fluctuation; RMSD, root mean square deviation; PMSF, phenylmethylsulfonyl fluoride; BisTris, 2-[bis(2-hydroxyethyl)amino]-2-(hydroxymethyl)propane-1,3-diol; Fmoc, *N*-(9-fluorenyl) methoxycarbonyl; LB, Luria-Bertani.

down studies (5, 6). Furthermore, ERAP1 has been shown to be able to regulate the immunogenicity of cancer cells, making it a potential target for cancer immunotherapy (7–9). ERAP1 is polymorphic, and several coding SNPs in its gene have been associated with predisposition to major human diseases, primarily related to inflammatory autoimmunity, often in epistasis with particular HLA alleles (10–12).

The role of ERAP1 in disease is believed to, at least in part, arise from its effects in shaping the cellular immunopeptidome (*i.e.* the sum of peptides that are presented by MHCI) (13). Several studies have described the effects of altered ERAP1 activity (either due to genetic manipulation or natural polymorphic variation) on the immunopeptidome of cell lines and *in vivo* models. ERAP1 has been found to influence a significant component of the immunopeptidome by altering both the sequence and length of presented peptides (14–17). These effects are generally interpreted to be the result of its aminopeptidase activity. *In vitro* analysis has revealed that ERAP1 has some unusual molecular properties compared with other aminopeptidases, which appear to fit well to this biological role. Specifically, peptide trimming appears to be affected by peptide sequence throughout the whole peptide and not just by the vicinity of the N terminus, where hydrolysis occurs (18). Furthermore, ERAP1 prefers to trim longer peptides over shorter ones, with the threshold being around 9 amino acids, the optimal length for binding onto MHCI (19, 20). The latter preference led to the "molecular ruler" mechanism proposal by Goldberg and colleagues in 2005 (21). All of those preferences are affected by polymorphic variation, possibly explaining the biological effects of ERAP1 haplotypes (22).

Apart from the well-characterized activity of ERAP1 to trim peptides in solution, an alternative mechanism has been proposed that offers a different vantage point on the generation of the immunopeptidome. According to this, ERAP1 can trim peptides while they are bound onto the MHCI. This mechanism has been supported by *in vitro* digestions using a covalently linked leucine-zipper dimer of ERAP1-ERAP2 (23) in addition to evidence from cellular assays (24, 25). The known ERAP1 crystal structures to date are largely incompatible with this mode of action due to steric hindrance that would make it difficult for ERAP1 to access the N terminus of an MHCI-bound peptide, which would be possible only for very long peptides, over 16 amino acids, even for the open ERAP1 conformer (19, 26). However, it is possible that ERAP1 conformations more open than those observed in structural studies to date might permit transient interactions with MHCI-bound peptides (27). Furthermore, as demonstrated in the recently solved cryo-EM structure of the peptide-loading complex (PLC, a multiprotein machinery that ensures proper loading of peptides onto MHCI), chaperone binding onto MHCI would make it difficult for ERAP1 to approach the MHCI, although ERAP1 interaction is not completely precluded by steric considerations (28, 29). In contrast, MHCI have been shown to protect peptides from degradation by ERAP1 (30). Partial dissociation of the MHCI-bound peptide in conjunction with conformational rearrangements of ERAP1 toward more open states has been proposed as a mechanistic requirement to overcome these limitations, but direct experimental tests are lacking (27, 31). Understanding the mode of ERAP1 peptide trimming is important because it alters our understanding of ERAP1's functional role in shaping the immunopeptidome *in vivo*. Solution trimming assumes that peptide selectivity arises from ERAP1-peptide interactions, whereas onto-MHCI trimming shifts at least part of the specificity to MHCI-peptide or ERAP1-MHCI-peptide interactions (26).

To provide insight into the mechanism of ERAP1 trimming of peptide precursors, we analyzed the ability of ERAP1 to trim several N-terminally extended antigenic peptide precursors in solution and in complex with the MHCI alleles HLA-B*58:01, HLA-B*08, and HLA-A*02. MHCI-peptide complexes with sequences extending from the N-terminal side of the binding groove and also MHCI-peptide complexes with internal bulges were examined. A combination of enzymatic, biochemical, and biophysical analyses suggests that whereas stably bound MHCI peptides are highly protected from ERAP1 activity, only the highly labile MHCI-peptide complexes can be apparently processed by ERAP1. This phenomenon is however more likely determined by fast dissociation of the peptide from the MHCI followed by ERAP1 processing in solution rather than by formation of an obligate ternary ERAP1-peptide-MHCI complex.

Results

*Trimming of extended peptide variants of the TW10 epitope bound to HLA-B*58*

Trimming by an aminopeptidase like ERAP1 requires access to a free N terminus of the peptide substrate. The vast majority of MHCI-peptide crystal structures, however, feature peptides that are 8–10 amino acids long and have the N terminus of the peptide making specific interactions within the MHCI-binding groove, interactions that are important for maintaining high binding affinity (32). One notable exception is the HIV Gag epitope TW10 (sequence TSTLQEQIGW) bound onto HLA-B*58:01 (henceforth referred to as B58), in which a recent crystal structure has shown that its N terminus protrudes from the peptide-binding groove (33). This configuration would allow N-terminal extension away from the MHCI, and therefore such peptides could be substrates of ERAP1. To test this, we prepared complexes of B58 with TW10 and a series of N-terminally extended peptides, up to 25 amino acids long, as shown in Fig. 1 (also see Fig. S1 for a representative chromatogram after *in vitro* folding). All peptides carry an N-terminal leucine, which is an optimal residue for trimming by ERAP1 and which facilitates monitoring of the trimming reaction by HPLC. In all cases, we were able to purify B58-peptide complexes and use them for trimming reactions. We compared trimming of the same molar concentration of peptide and B58-peptide complex, using two different enzyme concentrations. In all cases, we observed rapid degradation of the peptide in solution by ERAP1, but either very limited degradation or no degradation at all of B58-bound peptide (Fig. 1 and Fig. S2). A notable exception was the 25-mer peptide L-GW24, which was a poor substrate in solution (consistent with the known length dependence of ERAP1 activity (21)) and was not processed at all when bound onto B58. We thus conclude that most N-extended peptides based on the TW10 sequence are good ERAP1 substrates in solution, but all are very poor substrates when bound onto

Peptide (length)	Sequence
TW10	TSTLQEQIGW
L-TW10 (11)	Leu-TSTLQEQIGW
L-AW13 (14)	Leu-AGTTSTLQEQIGW
L-DW15 (16)	Leu-DIAGTTSTLQEQIGW
L-RW18 (19)	Leu-RGSDIAGTTSTLQEQIGW
L-MW22 (23)	Leu-MGSGGSGGSGGSTSTLQEQIGW
L-GW24 (25)	Leu-GQGGSGGSGGSGGSTSTLQEQIGW

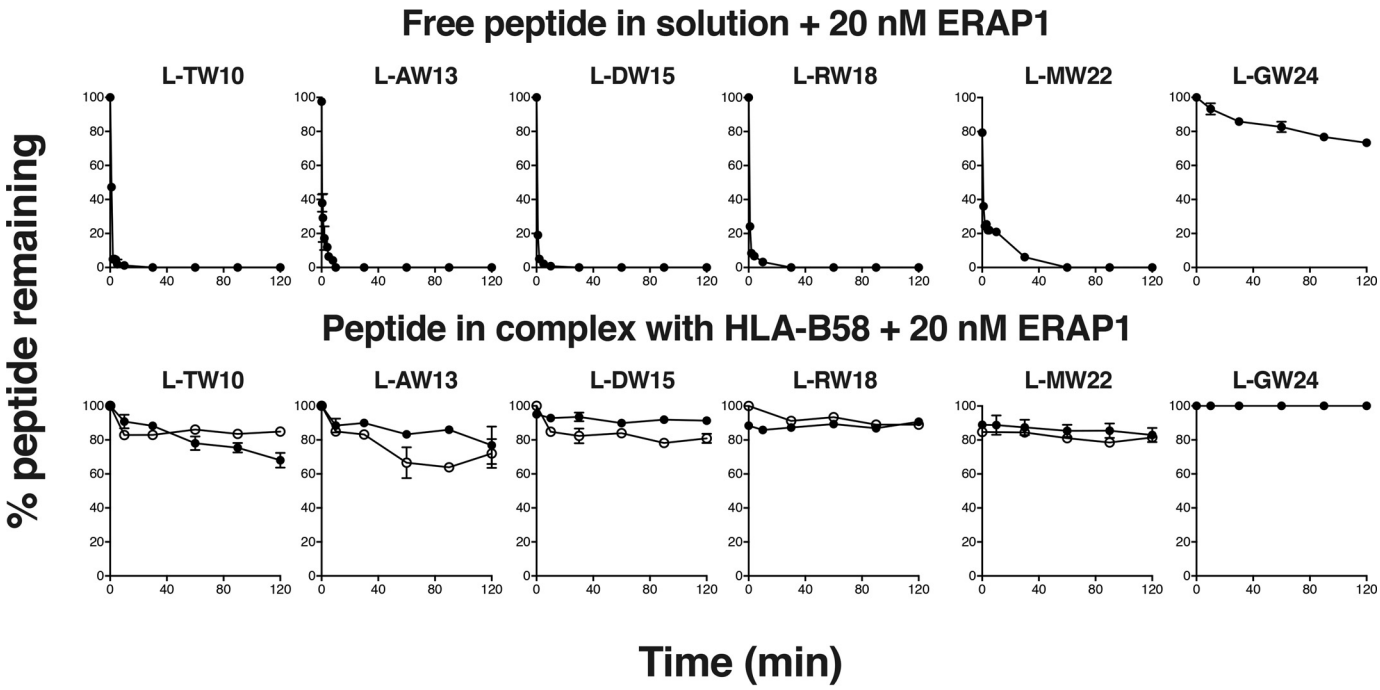

Figure 1. Trimming of peptides (10 μM) in solution and in preformed complexes with HLA-B58 (also 10 μM) by 20 nM ERAP1. *Top*, list of peptides used and their amino acid sequences. *Bottom*, percentage of remaining peptide after incubation with 20 nM ERAP1 as calculated by HPLC analysis. *Top panels*, peptide in solution; *bottom panels*, peptide in preformed complex with HLA-B58 (two replicates indicated by *filled* and *empty circles*).

B58. This suggests that although the N terminus of these peptides is exposed to the solvent when they are bound onto B58, ERAP1 is not able to form a catalytically productive complex.

Trimming of peptides bound on HLA-A02 in a bulged conformation

The majority of elongated peptides that are stably bound onto MHCI bind with a bulged conformation, as revealed by examining crystal structures deposited in the PDB database. In this conformation, the peptide N and C termini make atomic interactions with the MHCI, whereas the middle part of the peptide "bulges out" to allow the peptide to be accommodated within the limited length of the MHCI-binding groove (34). Two recent crystal structures of HLA-A*02 with a 15-mer and a 12-mer peptide epitope highlight this binding mode (35, 36). Because ERAP1 trimming has been implicated in the destruction of antigenic epitopes (3), we investigated whether ERAP1 can trim these two peptides (FK12 with the sequence FVLELEPEWTVK and FM15 with the sequence FLNKDLEVDGHFVTM) in solution and while bound onto HLA-A*02:01 (henceforth referred to as A02). Trimming was followed by MALDI-MS, an experimental approach that has the added benefit of being able to follow the generation of multiple trimming products. FK12 was a moderate substrate of ERAP1 in solution and was trimmed down to the 11-mer with a half-life of about 2 h (Fig. 2*A*). Strikingly, when bound onto A02, FK12 was processed very poorly, with less than 5% trimmed after 2 h (Fig. 2*D*). In contrast, FM15 was a good substrate of ERAP1, leading to 90% conversion to the 12-mer product after 30 min (Fig. 2, *B* and *C*). When in a preformed complex with A02, however, FM15 was processed much slower, with an estimated half-life of about 3 h (Fig. 2, *E* and *F*). We thus conclude that, similar to the results for B58, extended peptide epitopes bound onto A02 are protected by the activity of ERAP1 compared with trimming in solution.

*Trimming of extended peptides bound on HLA-B*08:01*

Considering that our results using B58 and A02 come in contrast with recent reports of ERAP1 trimming peptides while

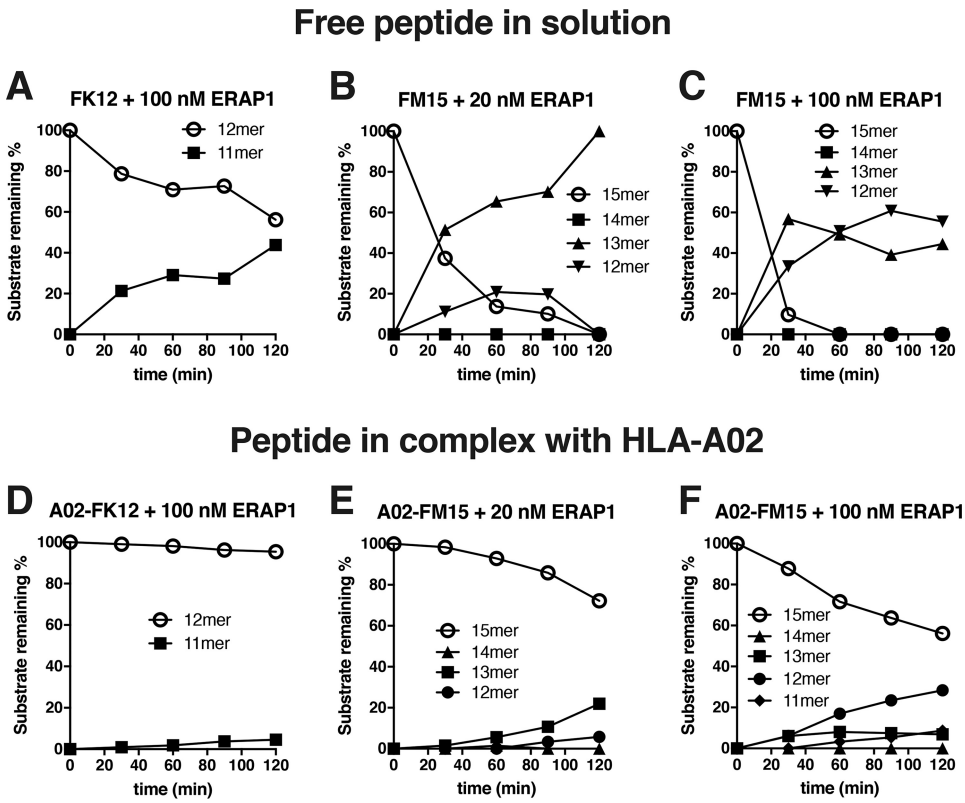

Figure 2. Trimming of FK12 and FM15 in solution (*top*; *A–C*) and in preformed complexes with A02 (*bottom*; *D–F*) followed by MALDI-MS.

bound onto HLA-B*08:01 (23, 37) (henceforth referred to as B08), we decided to examine whether this property is limited to the interaction of ERAP1 with this particular allele. Folding B08 with two 12-mers (sequence LSILLKHKKAAL, from nuclear factor NF-κB p105 subunit, henceforth called LL12 and sequence ARAALRSRYWAI, from nucleoprotein of influenza A virus, henceforth called AI12) was successful, based on size-exclusion chromatography followed by SDS-PAGE and MALDI-MS (Fig. S3). In solution, LL12 was found to be an exceptionally good substrate for ERAP1 and was converted to the 11-mer with a half-life of 19 ± 5 min (Fig. 3*A*). Similarly, LL12 was found to be a good substrate for the homologous aminopeptidase ERAP2, an enzyme also described to play roles in antigen processing (38). In sharp contrast, LL12, in preformed purified complex with B08, was completely resistant to trimming by either ERAP1 or ERAP2, even when the enzyme was used at concentrations up to 100 nM (Fig. 3*B*). We conclude that in accordance with the results obtained for B58 and A02, elongated peptide LL12 binding onto B08 can fully protect it from trimming by ERAP1.

Trimming of the peptide AI12 by ERAP1 in solution was found to be very efficient and dependent on enzyme concentration (ranging from 2 to 100 nM, as shown in Fig. 4*A*). Under most conditions, trimming by ERAP1 led to the accumulation of the 9-mer antigenic epitope ALRSRYWAI (henceforth called AI9; Fig. 4*A*, *top row*). At the highest concentration of ERAP1 (100 nM), however, the 12-mer peptide was fully consumed within 5 min, and even the 9-mer epitope was trimmed down to shorter peptides (Fig. 4*B*). These observations are consistent with the dual nature of ERAP1 in being both a producer and a destroyer of antigenic epitopes (3). The AI12 peptide was also found to be a good substrate of the homologous aminopeptidase ERAP2, and this was also the case for leucine aminopeptidase (LAP), a cytosolic metabolic enzyme not directly associated with antigen processing (39). The effect of LAP and ERAP2, however, was the accumulation of smaller peptides, notably the 6-mer, which is consistent with the proposed role of ERAP2 in destroying antigenic epitopes (40).

Strikingly, when analyzing the reaction of preformed complexes of AI12 with HLA-B08, we observed significant trimming by ERAP1, which depended on the enzyme concentration (Fig. 4*A* (*bottom row*) and Fig. S4). Trimming rates of the 12-mer, however, appeared to plateau at 100 nM concentration of enzyme and were always much lower compared with trimming in solution (Fig. 4*C*). Furthermore, trimming of B08/AI12 by ERAP1 appeared to be less efficient in generating the mature epitope (9-mer) than trimming in solution. Still, this was the first time in our analysis that we recorded significant trimming of a preformed MHCI-peptide complex, and this appears to support the notion that the interaction of ERAP1 with B08 is different when compared with A02 and B58. This phenomenon, however, was not unique to ERAP1, as both ERAP2 and LAP were able to trim the preformed B08/AI12 complex at rates comparable with ERAP1.

To better understand the effects of ERAP1 on B08 complexes, we analyzed the behavior of those complexes by native PAGE (Fig. 4*B* and Fig. S5). The various B08 complexes migrate differently in native PAGE, depending on the total charge carried by different peptides, allowing us to follow the conversion from one complex to another over time (Fig. S5*A*). Complexes

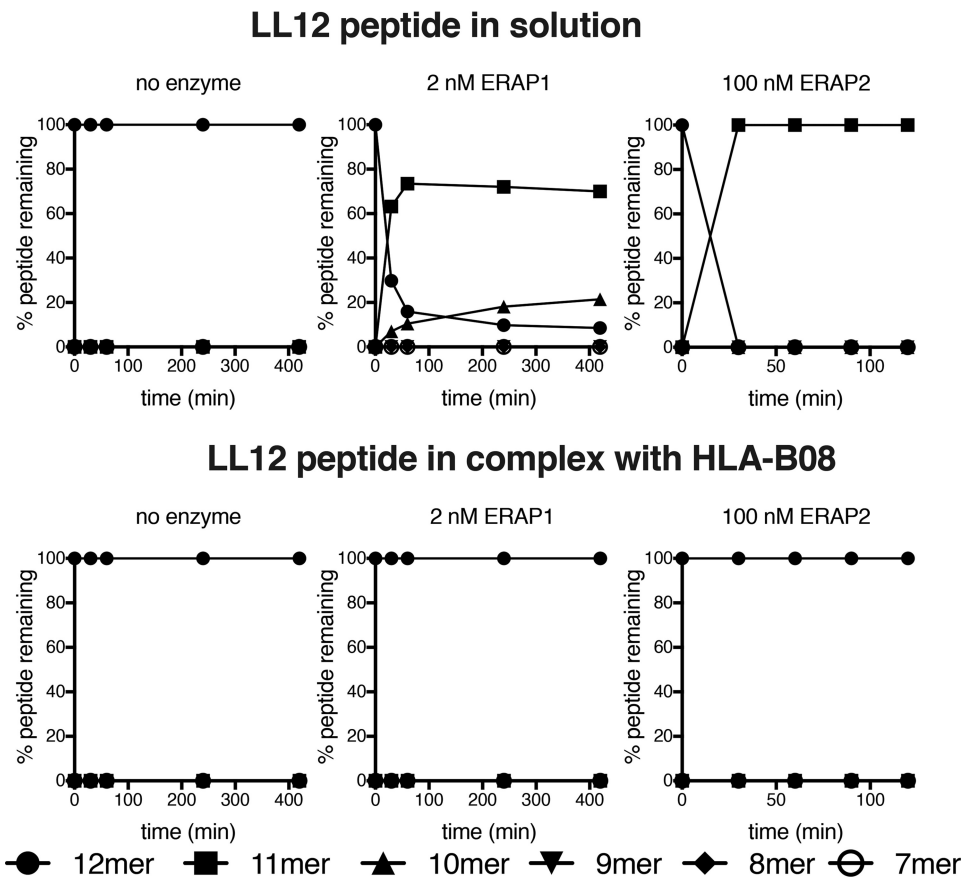

Figure 3. Trimming of LL12 in solution (*top*) and in preformed complexes with HLA-B*08 (*bottom*), by ERAP1 and ERAP2.

with the 9-mer epitope EI9 and the 12-mer peptide LL12 were stable upon incubation with ERAP1 (Fig. 4*B* (*left*) and Fig. S5). In contrast, incubation of the complex B08/AI12 with ERAP1 or ERAP2 resulted in the downshift of the protein band, corresponding to complexes of B08 with smaller peptides (Fig. 4*B* (*middle* and *right*) and Fig. S5). The rate of change in migration depended on the amount of enzyme added. Adding the epitope AI9 in the complex allowed us to measure the rate of exchange of each 12-mer for the 9-mer epitope (Fig. S5, *J* and *K*). Using densitometric analysis, we calculated the rate of conversion for each reaction (Fig. 4*D*). Similar to the results from the MALDI-MS analysis, both ERAP1 and ERAP2 were able to convert the initial 12-mer complex to MHC complexes with smaller peptides, displaying kinetics that plateaued around 100 nM ERAP1. In all cases, the exchange of AI12 for AI9 was faster. We conclude that although ERAP1 appears to be able to trim the 12-mer peptide AI12 in preformed B08/AI12 complexes, this reaction appears to be slower than the dissociation rate of AI12 from B08 when in competition with the AI9 epitope.

Characterization of thermodynamic and kinetic stability of B08 complexes

The sharp difference between the behavior of the two B08 complexes (with the AI12 *versus* the LL12 peptide) in regard to trimming by ERAP1 prompted us to characterize further their thermodynamic and kinetic stability. Whereas both 12-mers formed complexes with B08 that were sufficiently stable to allow characterization (Fig. S3), biophysical analysis suggested that the complexes are quite distinct in terms of thermodynamic and kinetic stability (Fig. 5*A* and Fig. S6 and Tables S1 and S2). Using the differential scanning fluorimetry assay (DSF) (41), the B08/LL12 complex displayed a T_m value of 57.7 ± 0.4 °C. In contrast, the B08/AI12 complex was markedly less stable with a T_m value of 47.8 ± 2.3 °C. For comparison, analysis of B08 in complex with the antigenic peptide ELRSRYWAI (EI9) and its analogue ALRSRYWAI (AI9) indicated T_m values of 66.1 ± 0.3 and 63.3 ± 0.8 °C, respectively. Measurements of their thermodynamic stability using CD gave similar comparative results. Additionally, kinetic stability as judged by exchange of the peptide with excess SYPRO Orange dye was very different for the two peptides (Fig. 5, *B–G*). The B08/LL12 complex was found to be reasonably stable with a half-life of 362 min, which is comparable with the half-lives of 891 ± 92 and 1056 ± 152 min that were determined for the 9-mer antigenic peptide complexes B08/EI9 and B08/AI9, respectively. In contrast, B08/AI12 was kinetically labile, with an estimated half-life of 9 ± 1 min (Fig. 5, *E* and *F*). These results were in good agreement with native-PAGE analysis of folded complexes in competition with excess free epitope AI9, which showed half-lives of 317 min for B08/LL12 and 18 min for B08/AI12 (Fig. S5, *J* and *K*). Taken together, these results suggest that whereas both N-terminally extended peptides can form sufficiently stable ternary complexes with B08 to allow their purification, AI12 forms a significantly more kinetically labile and thermodynamically unstable complex compared with LL12.

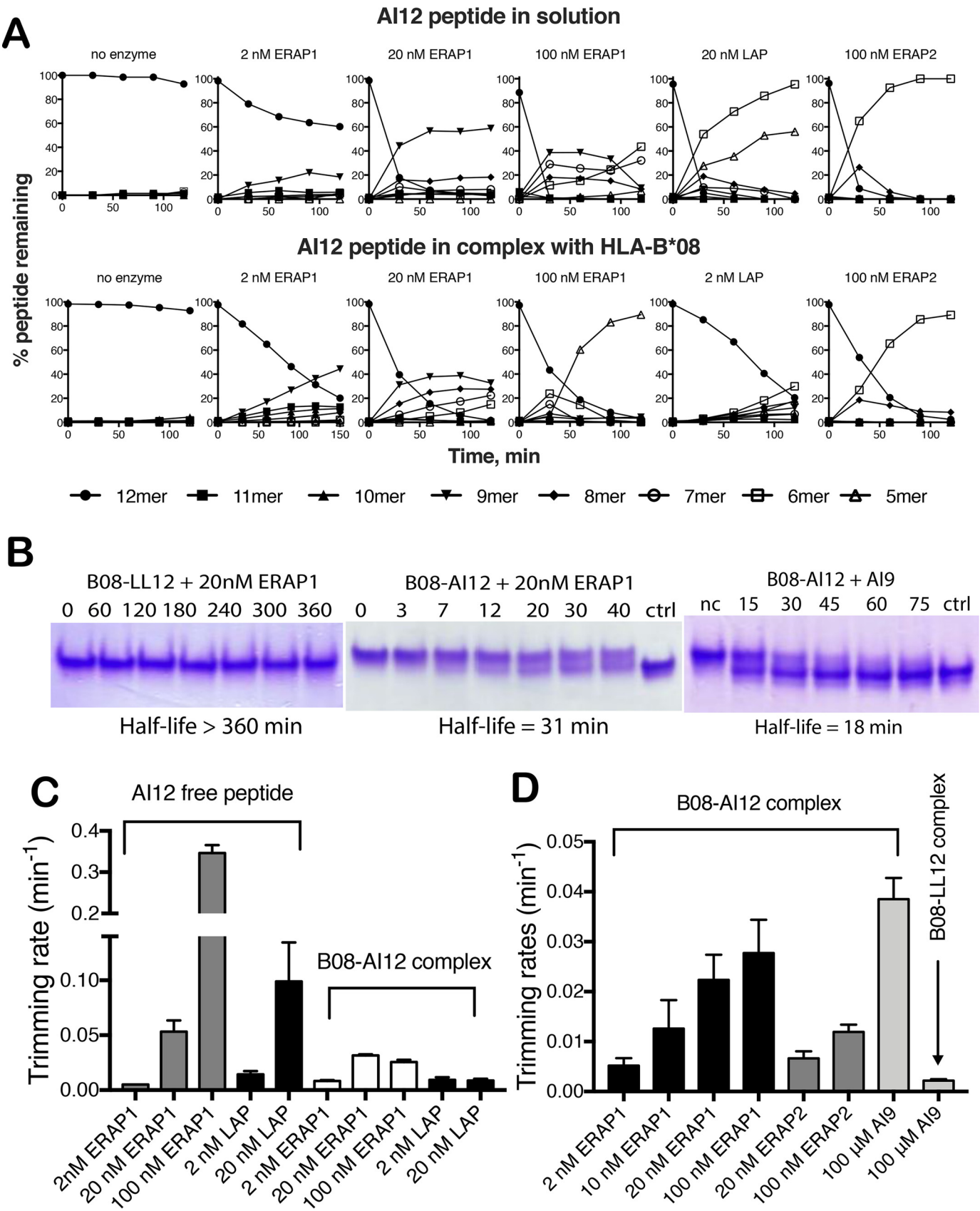

Figure 4. *A*, trimming of AI12 in solution and in preformed complexes with HLA-B08, by ERAP1, ERAP2, and LAP followed by MALDI-MS. *B*, changes in mobility in native PAGE of HLA-B08/12-mer peptide complexes upon incubation with ERAP1 or 9-mer peptide. *Numbers* indicate incubation time in minutes. Gels are also shown in Fig. S5 as part of a complete series. *C*, calculated trimming rates of 12-mer peptide AI12 from MALDI-MS experiments. *D*, calculated peptide exchange rates from native-PAGE experiments. *Error bars*, S.D.

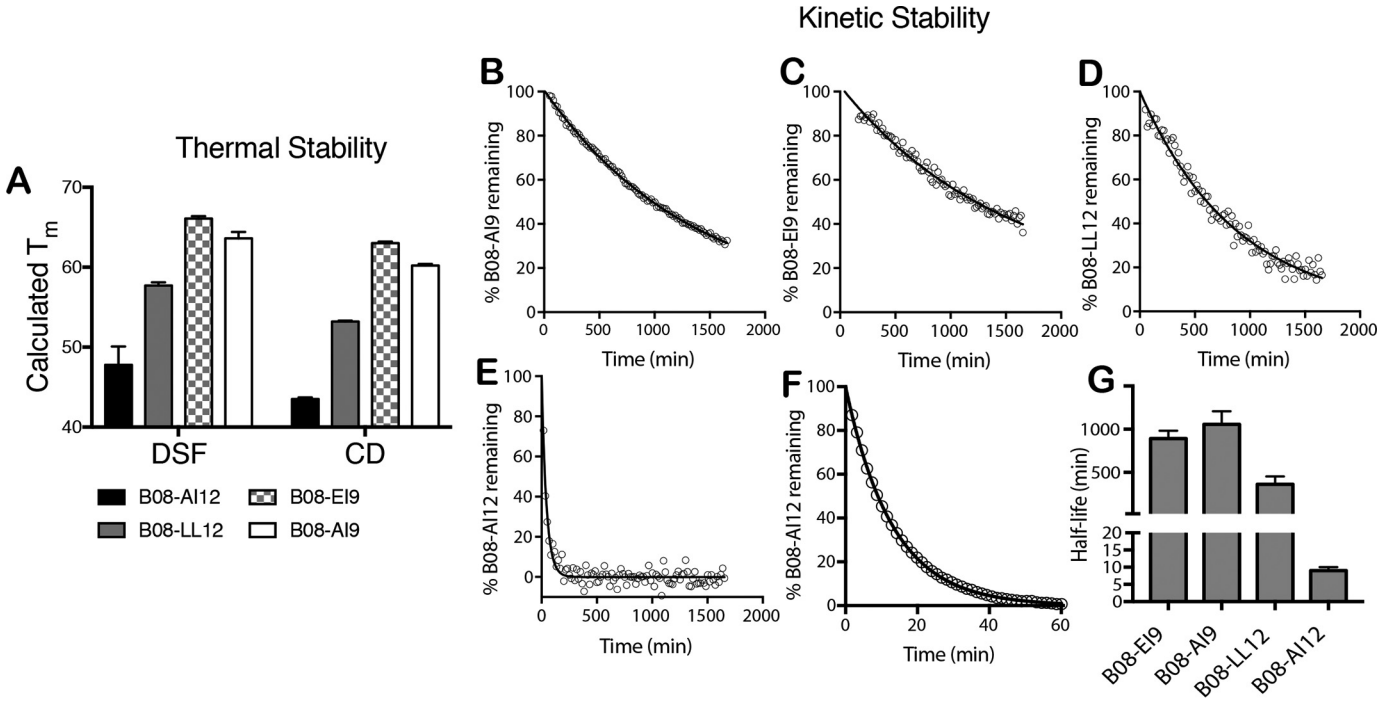

Figure 5. *A*, T_m values of four HLA-B08 complexes calculated by differential scanning fluorimetry assay and CD. Both approaches reveal the same pattern in relative thermodynamic stabilities, although absolute values are lower for CD measurements, possibly due to slower scanning rates, as shown previously (51, 71). *B–F*, kinetics graphs describing the dissociation of bound peptide off of HLA-B08 during competition by the SYPRO Orange dye. *G*, calculated half-lives of dissociation for each peptide. *Error bars*, S.D.

Molecular dynamics of MHCI-peptide complexes

To gain atomic-level insight into the role of the N terminus extension for the less stable B08/AI12 complex as compared with the more stable B08/LL12, we carried out a comparative molecular dynamics (MD) study. For reference, we also performed MD simulations for the complexes of the 9-mer antigenic peptides EI9 and AI9 using the recent X-ray crystal structure of B08 complex with EI9 (PDB code 5WMQ, resolved at 1.4 Å) (42). The modeling of the N-terminally extended peptides was based on the hypothesis that the peptides would bulge out to favorably accommodate their N and C termini within the binding groove of the MHCI, similar to the analyzed A02 complexes. Starting from AI12, we used the X-ray coordinates of residues P1 (E) and P4–P9 (SRYWAI) as template for the modeling of the 12-mer peptide, so as to constrain the position of the N terminus inside pocket A of the HLA-B08. Five models with variable conformations at the "bulged-out" region of AI12 were selected as starting structures for the MD simulations (Fig. S7). These conformations were used as templates for the modeling of LL12, to compare the sampled conformational space of AI12 with LL12 with initial conditions as similar as possible (Fig. S8).

For the four B08-peptide systems, we performed five MD simulations of 500 ns each, from which we calculated the mean atomic root mean square fluctuation (RMSF) values of the C^{α} atoms of the peptides, after root mean square fitting of the trajectories with respect to the antigen-binding domain (C^{α} atoms of residues 1–180) of the MHCI (Fig. 6). The 9-mer epitope EI9 and the homologue AI9 peptide displayed the highest stability, with the lowest mean RMSF values (<0.9 Å), followed by LL12, for which the RMSF values were 0.9–1.8 Å throughout the whole sequence (Figs. S9–S11). In contrast, AI12 exhibited very high mobility at the three N-terminal residues (Fig. 6), with progressively lower values toward the C terminus of the peptide (Fig. 6). The high flexibility of AI12 was a result of partial dissociation of the N terminus from pocket A of the MHCI, whereas the five C-terminal residues (RYWAI) were as stable as in the 9-mer peptides (Figs. S11 and S12). To confirm that this effect is not dependent on the initial conformation of the peptide employed, we carried out five additional MDs for each B08 complex with AI12 and LL12, starting from the conformation that displayed the most stable complexes in our simulations (designated as "sim-2" in Figs. S9–S11). In accordance with the first set of simulations that were initiated from different peptide conformations, AI12 revealed significantly higher mobility at the N-terminal residues with respect to LL12 (Fig. S13). This observation is in good agreement with the results of the thermal and kinetic stability measurements for the four HLA-B08–peptide complexes (Fig. 5), with the experimental T_m and half-life values correlating nicely with the trend of the mean RMSF values for EI9 ≈ AI9 < LL12 ≪ AI12. Although the MD simulations at the microsecond timescale cannot be directly translated to the much longer timescales of the experimental measurements, our results suggest that the kinetic instability of B08/AI12 as compared with B08/LL12 is probably a result of the highly labile N terminus moiety of AI12 that can readily detach from the MHCI-binding groove.

No evidence for a ternary ERAP1-MHCI-peptide complex when using a transition-state analogue pseudopeptide trap

Transition-state analogues have been used as potent tools to study enzyme-substrate interactions. In particular, phosphinic

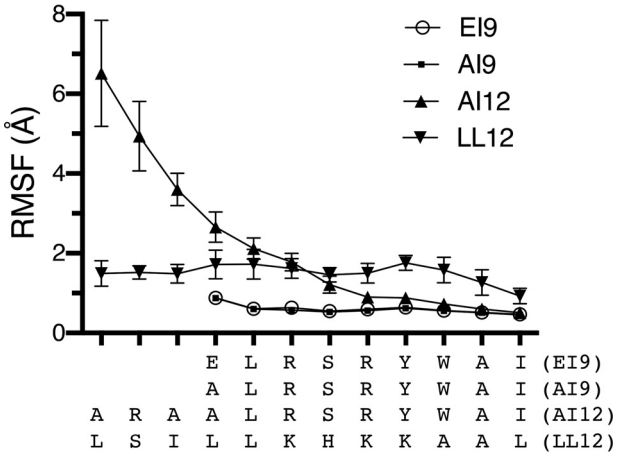

Figure 6. Plots of the root mean square fluctuations from the average position of the C^{α} atoms of the peptides EI9, AI9, AL12, and LL12 as calculated from the MD simulations of the B08-peptide complexes. The values given for each residue are mean values from five 500-ns MD simulations with *error bars* showing the S.E.

pseudopeptides have been shown to be valuable tools for the study of ERAP1 and ERAP2 interactions with peptide substrates because they are nonhydrolyzable and feature high affinities for the active site of those aminopeptidases (40, 43). Based on the observation that ERAP1 appears to trim the peptide AI12 in preformed complex with B08, we wanted to test the possibility that ERAP1 might be forming a transient complex with the MHCI-peptide complex. To probe this putative interaction, we designed a phosphinic pseudopeptide based on the sequence of AI12. The peptide H-AΨ(P(O)(OH)CH_2)KAALRSRYWAI-OH, named DG078, carries the phosphinic group in place of the N-terminal peptide bond, which is nonhydrolyzable and is expected to bind to the active site of ERAP1 with high affinity as previously shown for other similar peptides (40, 44). DG078 was successfully folded with B08 at a similar yield as AI12, and the presence of the peptide in the purified complex was confirmed by MALDI-MS (Fig. S14). Thermal stability analysis revealed a T_m value of 46.1 ± 0.3 °C, which is similar to that of B08/AI12, indicating that the introduction of the phosphinic moiety did not significantly alter binding onto B08 (Fig. S15). Furthermore, the dissociation rate of the peptide off B08 upon competition with SYPRO Orange had a half-life of 12.7 min (Fig. 7*A*), which is similar to the half-life calculated for AI12 (9 min). As expected, DG078 in solution acted as a potent inhibitor of ERAP1 with a calculated IC_{50} value of 39 nM (Fig. 7*E*). Given the high affinity of DG078 for both ERAP1 and B08, we hypothesized that it may be an efficient linker to enhance any potential transient interactions between ERAP1 and B08. To investigate this, we analyzed B08 in complex with DG078 using native PAGE, either alone or premixed with ERAP1 or ERAP2 (Fig. 7*B*). Surprisingly, we were unable to detect any stable heterotrimeric species consisting of ERAP1/DG078/B08, suggesting that ERAP1 cannot interact stably with DG078 while the peptide is bound to B08.

Because this finding raised questions regarding how ERAP1 can appear to trim AI12 while it is bound onto B08, we further analyzed the interaction of ERAP1 with DG078 by following the enzymatic activity of ERAP1 (Fig. 7*C*). As expected, mixing 500 nM DG078 with 10 nM ERAP1 greatly reduced ERAP1's ability to hydrolyze the fluorigenic substrate leucine-aminomethylcoumarin (Fig. 7*C*). Interestingly, using 500 nM of B08/DG078 had a similar effect on ERAP1 activity, indicating that DG078, from preformed B08 complexes, could access the active site of ERAP1. Titrating B08/DG078 to ERAP1 revealed a dose-dependent decrease of its activity, with an apparent IC_{50} of 167 nM, which is about 5-fold weaker than for the free DG078 peptide (Fig. 7*E*). Notably, the inhibition of ERAP1 by B08/DG078 showed a much smaller slope compared with free DG078, suggestive of a more complex kinetic phenomenon. Strikingly, these effects were not limited to ERAP1, as 500 nM DG078 as well as B08/DG078 were able to inhibit LAP (Fig. 7*C*, *right*). DG078 was able to inhibit LAP with an IC_{50} that was lower than for ERAP1 (108 nM; Fig. 7*E*), but B08/DG078 inhibited LAP with a similar IC_{50} of 152 nM (Fig. 7*E*).

In summary, our experiments suggest that DG078 from preformed complexes with B08 can access ERAP1's active site, but cannot form stable ternary complexes. This apparent paradox can be reconciled by taking into account the fast off kinetics of DG078 from B08. It is therefore possible that the DG078 peptide dissociates from the B08/DG078 complex to interact with and inhibit ERAP1. It should be noted that because of the 50-fold excess of DG078/B08 complex used in those experiments and the high affinity of DG078 for ERAP1, even a minor population of dissociated DG078 from the B08/DG078 complex would be sufficient to fully inactivate the enzymes. By extrapolation, it is therefore highly probable that the apparent trimming of AI12 while bound onto B08 is a result of rapid peptide dissociation and subsequent solution trimming, rather than the formation of a ternary ERAP1/B08/AI12 complex.

No evidence for direct molecular interactions between ERAP1 or ERAP2 and the peptide-loading complex

Peptide loading onto MHCI inside the ER is facilitated and regulated in cells by a multiprotein complex called the PLC (45). A recently solved structure of the PLC revealed how all of its protein components cooperate in a single molecular entity (29). ERAP1 and ERAP2 were not found to be part of this complex, although transient interactions could not be ruled out. Because we found no evidence for a direct ERAP1-MHCI interaction, we decided to investigate possible interactions between ERAP1 or ERAP2 and a preformed PLC. To this end, PLC was purified via ICP47-SBP from Raji cells and incubated for 30 min at 4 °C bound onto streptavidin-coated beads with a 4-fold excess of ERAP1 or ERAP2 or a mixture of both (Fig. 8*A*). The beads were then washed, and bound proteins were eluted and analyzed on SDS-PAGE (Fig. 8*B*). All of the components of the PLC can be visualized on the gel (TAP1/2, ERp57, calreticulin, tapasin, MHCI heavy chain, and β_2-microglobulin) after elution from the beads. However, no ERAP1 or ERAP2 could be detected on the beads, whereas both enzymes were found in the wash fraction only. This result was confirmed by size-exclusion chromatography (SEC) that indicated discrete single monodisperse peaks for both the PLC and ERAP1 or ERAP2, which were not significantly altered when the PLC and ERAPs were preincubated together (Fig. 8, *C–E*). This analysis suggests that neither

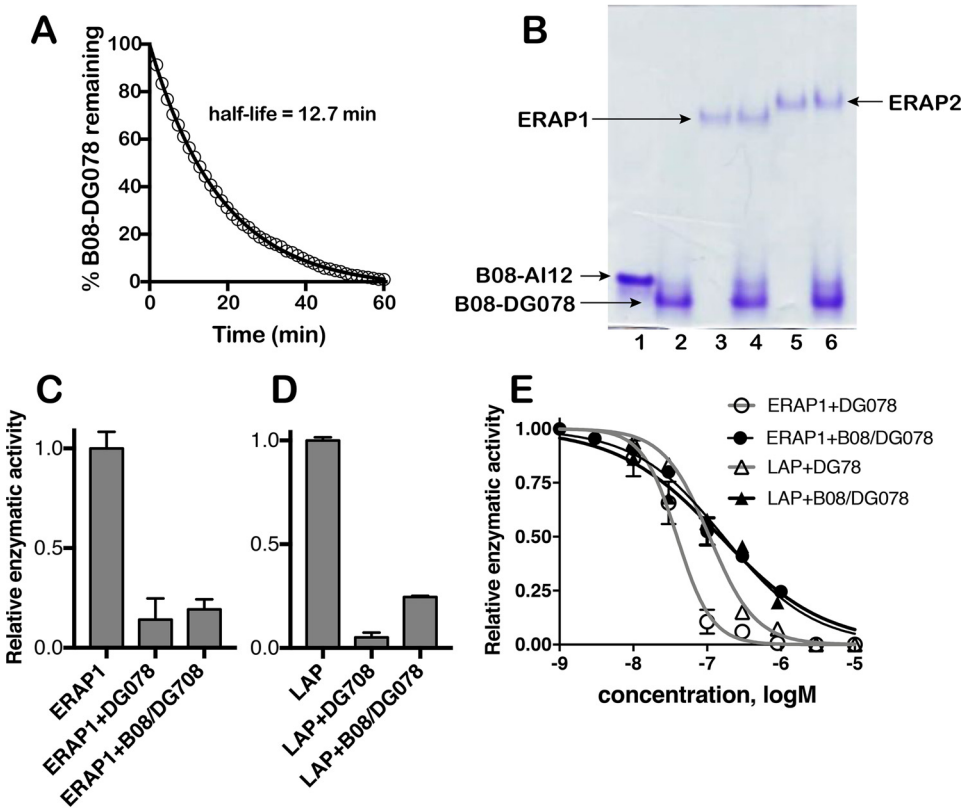

Figure 7. *A*, dissociation of DG078 from HLA-B08 during competition with SYPRO Orange. *B*, native-PAGE analysis of HLA-B08 and ERAP mixtures. *Lane 1*, 1 μg of B08/AI12 complex; *lane 2*, 1 μg of B08/DG078 complex; *lane 3*, 2 μg of ERAP1; *lane 4*, 1 μg of B08/DG078 mixed with 2 μg of ERAP1 (1:1 molar ratio); *lane 5*, 2 μg of ERAP2; *lane 6*, 1 μg of B08/DG078 mixed with 2 μg of ERAP2 (1:1 molar ratio). *C* and *D*, relative enzymatic activity of ERAP1 (*left*) and LAP (*right*) upon the addition of 500 nM DG078 or HLA-B08/DG078 complex. *E*, enzymatic activity of ERAP1 or LAP upon titration of DG078 of HLA-B08/DG078 complex. *Solid lines*, fits to a four-parameter dose-dependent inhibition model as described under "Experimental procedures." *Error bars*, S.D.

recombinant ERAP1 nor ERAP2 can form stable interactions with preformed PLC isolated from cells.

Because it is possible that ERAP1 and ERAP2 can form transient interactions with the PLC as they catalyze trimming of an MHCI-bound peptide, we designed an N-terminally extended 15-mer peptide trap that could stabilize this transient interaction. Peptide DG057 is based on the epitope SQFGGGSQY from the eukaryotic translation initiation factor 3 subunit D, which is an optimal ligand for HLA-A03 that is the MHCI allele component of PLC purified from Raji cells (29). DG057 carries a phosphinic group between the first two amino acids, similarly to the peptide DG078 used in Fig. 7, and should act as a nonhydrolyzable, transition-state, high-affinity inhibitor for both ERAP1 and ERAP2. We therefore hypothesized that this peptide could operate as a molecular trap that can stabilize a transient interaction between ERAP1 or ERAP2 and the PLC. Indeed, DG057 was found to be a potent inhibitor of ERAP1 and ERAP2 *in vitro*, with an IC_{50} of 20 and 648 nM, respectively (Fig. S16). As described before, PLC purified via ICP47-SBP from Raji cells was bound on streptavidin-coated beads (Fig. 8*A*) (29). First, either the PLC or ERAP1, ERAP2, or premixed ERAP1 and ERAP2 were incubated with DG057 for 30 min. Afterward, the PLC was incubated for 30 min with either 1) ERAP1, ERAP2, or ERAP1/ERAP2 mixture only or 2) ERAP1, ERAP2, or ERAP1/ERAP2 mixture preincubated with DG057. Additionally, DG057-incubated PLC was incubated with ERAP1, ERAP2, or ERAP1/ERAP2 mixture. The beads were then washed with buffer, and bound proteins were eluted and analyzed on SDS-PAGE (Fig. 8*B*). All components of the PLC were detected bound onto the streptavidin beads, but neither ERAP1 nor ERAP2 were found in the pulldown. In contrast, ERAP1 and ERAP2 were only detected in the wash fraction (supernatant). SEC analysis of the same conditions confirmed this result. The migration behavior of the PLC or ERAP1/2 was not altered after peptide incubation and treatment with ERAP1 (Fig. 8*C*), ERAP2 (Fig. 8*D*), or ERAP1/2 mixture (Fig. 8*E*). Also, the addition of DG057 did not alter the migration behavior of any of the protein components. This analysis suggests that even in the presence of a nonhydrolyzable peptide analogue trap for ERAP1 or 2, no stable molecular complex between ERAP1 or ERAP2 and the PLC could be detected.

Discussion

A detailed understanding of how ERAP1 trims antigenic peptide precursors is potentially of critical significance, as it can alter our understanding of the generation of the cellular immunopeptidome. Several studies have already demonstrated significant effects of ERAP1 down-regulation on the immunopeptidome of cells and have associated these changes with alterations of adaptive immune responses in autoimmunity and cancer (13). Furthermore, pharmacological regulation of ERAP1 activity is an emerging approach for cancer immunotherapy, and thus a deep mechanistic knowledge of how

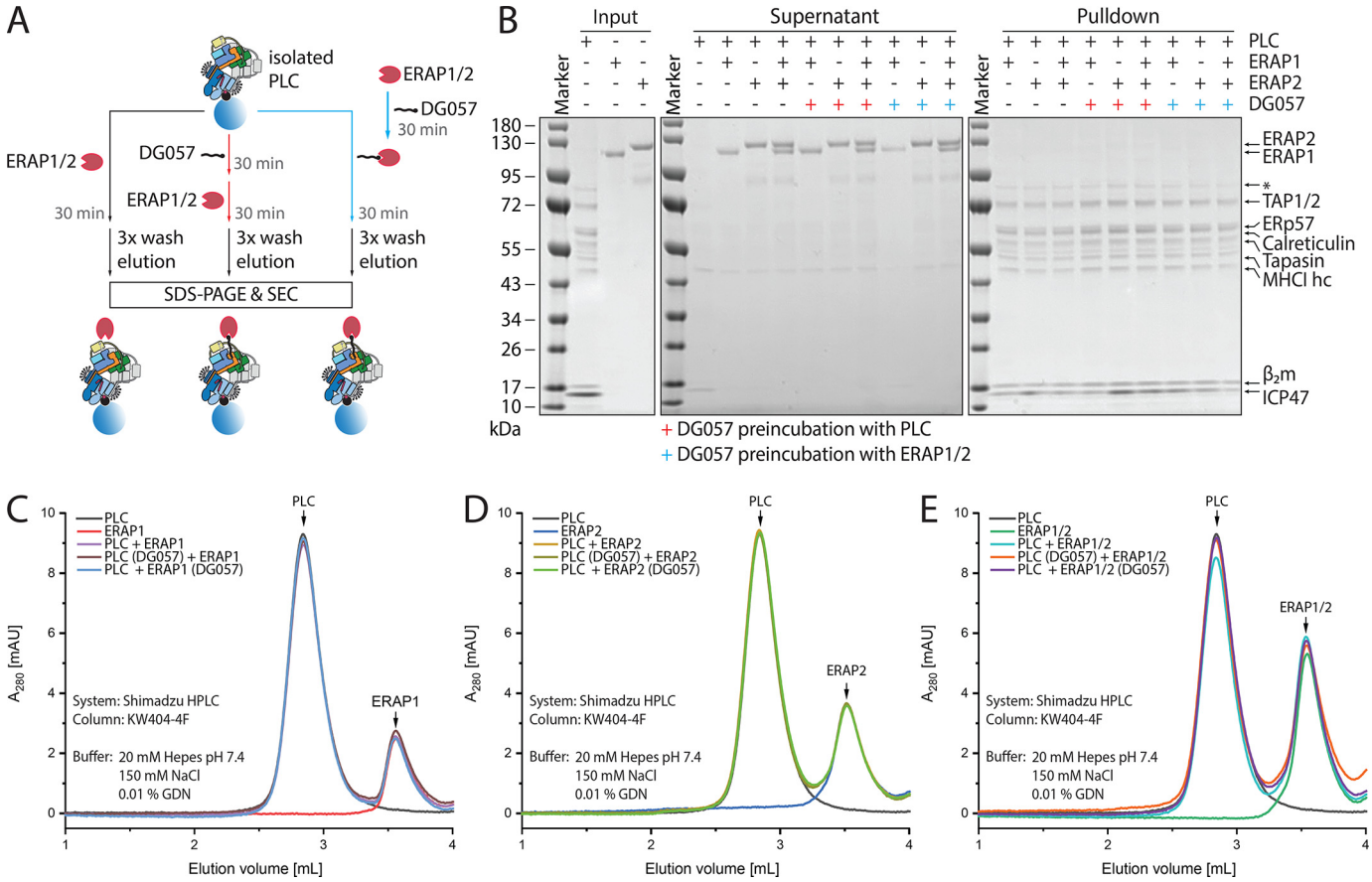

Figure 8. Investigation of the molecular interactions between ERAP1 or ERAP2 with fully assembled native PLC. *A*, *schematic illustration* of ERAP1 or ERAP2 pulldown with PLC (*left*) and DG057-preloaded PLC (*middle*) and pulldown of DG057-preloaded ERAP1 or ERAP2 (*right*). *B*, SDS-PAGE analysis of PLC bound onto streptavidin beads incubated with ERAP1, ERAP2, and ERAP1/ERAP2 mixture in the absence or presence of peptide DG057. *C–E*, overlay of chromatograms from size-exclusion analysis of mixtures of PLC and ERAP1 (*C*), ERAP2 (*D*), and ERAP1/ERAP2 mixture (*E*) in the presence or absence of peptide DG057. The PLC elutes as a single monodisperse peak at 2.85 ml, and ERAP1 and ERAP2 elute as single peaks at 3.58 and 3.53 ml, respectively. ERAP1/ERAP2 mixture elutes at 3.55 ml. Premixing PLC with ERAP1 and/or ERAP2 does not significantly change the migration of the PLC or ERAP1 or ERAP2. The addition of peptide DG057 to ERAP1 or ERAP2 and/or the PLC does not significantly change the migration of the proteins.

ERAP1 regulates the immunopeptidome is crucial for optimizing potential therapies (46, 47).

Two main pathways of ERAP1-mediated antigenic peptide generation have been proposed in the literature (26). In one, solution trimming of antigenic peptide precursors precedes MHCI loading, whereas in the second, peptides are first bound onto MHCI and are then trimmed by ERAP1. For the second pathway, two distinct submechanisms can be envisaged: 1) ERAP1 trims peptides that overhang away from the MHCI without any atomic interactions with the MHCI, and 2) ERAP1 trims peptides while making specific atomic interactions with the MHCI that help orient it toward the peptide and guide trimming. Whereas these pathways and mechanisms are not mutually exclusive, they present key differences in how ERAP1 recognizes and selects its substrates. Solution trimming, as a well-established mechanism for M1 aminopeptidases, requires enzyme-peptide interactions between the N terminus of the peptide and the active site, which, in the case of ERAP1, may extend to the whole length of the peptide (18, 21). Indeed, recent high-resolution crystal structures of ERAP1 with peptide analogues revealed extensive interactions between the peptide and a large internal cavity in the enzyme where the substrate is sequestered during the catalytic cycle (19, 48, 49). In addition, a specific interaction between the C terminus of the peptide and a regulatory site of ERAP1 was found to be important for longer peptides (49). In contrast, on-MHCI trimming necessitates that at least some interactions remain between MHCI and the peptide, at a minimum between the C terminus of the peptide and the F-pocket of the MHCI antigen-binding groove (31). Additionally, loss of ERAP1-peptide interactions may be substituted with ERAP1-MHCI interactions that could enhance peptide-trimming rates. Whereas most MHCI-peptide crystal structures known to date have the peptide N terminus tightly bound to the MHCI, some notable exceptions exist, which demonstrate how the peptide N terminus can extend away from the MHCI and thus be vulnerable to trimming by an aminopeptidase (33, 50). This was recently demonstrated with a series of extended peptides bound onto HLA-B08 (37). In contrast, formation of a transient ERAP1-MHCI trimming complex would necessitate conformations not previously observed experimentally, but simulated computationally (27, 31). To date, no direct ERAP1-MHCI protein-protein interactions have been demonstrated (26).

Here, we investigated ERAP1-mediated trimming in different cases of antigenic peptide precursors in solution and in complex with MHCI alleles HLA-B*58, HLA-B*08, and HLA-A*02. We tested peptides in MHC complexes where both of the

peptide termini are buried within the binding groove, peptides that have different length central bulges, and peptides in MHCI complexes where the N terminus extends away from the groove at variable lengths. Our aim was, on the one hand, to test the generality of previous studies that suggested on-MHC trimming (23, 31) and, on the other hand, to test the relative kinetics of the two mechanisms, something that has not been addressed before. Kinetic analysis is critical to a detailed understanding of enzyme function, given that rates will determine whether a particular reaction is relevant in a biochemical pathway. We find that in all cases tested (11 different peptide sequences and their various length variants and three HLA alleles), MHCI binding protects rather than facilitates ERAP1 trimming, similar to what was demonstrated before for a murine MHCI (30). Of the antigenic peptide precursors tested, only one 12-mer, when bound to HLA-B*08, was found to be trimmed at apparent rates that were within the same order of magnitude as solution trimming. This was in sharp contrast to another 12-mer that when bound to the same allele was completely protected from ERAP1. Biophysical analysis suggested that these two 12-mers differ greatly in thermodynamic stability and that the 12-mer which was susceptible to ERAP1 is very labile and can rapidly dissociate from MHCI, at rates faster than the fastest recorded rate of ERAP1 trimming for this peptide. Indeed, on-MHCI trimming for this peptide was in all cases slower than the dissociation rate, suggesting that the observed trimming could be explained by a two-step mechanism that depends on rapid dissociation and subsequent solution trimming steps. This would suggest that previous observations of apparent on-MHC trimming were limited to the particular combination of MHCI allele-peptide tested and were likely due to the dynamic nature of the peptide-MHCI complex rather than a specific ERAP1-MHCI interaction.

Although ERAP1 has been extensively studied for its ability to generate antigenic peptides from N-terminally elongated precursors, it can also overtrim antigenic peptides to lengths not suitable for binding onto MHCI, essentially destroying the epitope (3). Recent analysis of the effect of ERAP1 on the immunopeptidome of cells has suggested that the destructive properties of ERAP1 may have been underestimated and could actually be the dominant function of the enzyme (47, 52, 53). The data presented herein highlight the ability of MHCI to protect peptides from ERAP1-mediated degradation and are thus consistent with the hypothesis that ERAP1 acts to limit available peptides for MHCI.

Since the discovery of ERAP1, several studies have recognized its specialized function in processing antigenic peptides (54). Indeed, *in vitro* analyses have revealed that ERAP1, like other related aminopeptidases, has preferences for the peptide N terminus (55, 56), but, unlike other related aminopeptidases, it also has preferences for peptide length and sequence (18, 20, 21), including the C terminus of the peptide (21). Recently solved high-resolution crystal structures of ERAP1 with peptide analogues have provided insight into the atomic basis of these properties by identifying a regulatory site that is responsible for recognition of the C terminus of elongated peptides (49). The homologous ERAP2 does not share the length preferences and C-terminal recognition properties of ERAP1, consistent with a discrete role in antigen processing (38, 40). Additionally, LAP does not have any length or internal sequence preferences (20). Therefore, if the primary mechanism of ERAP1-mediated trimming included the recognition of the MHCI-peptide complex as a substrate, one might expect ERAP1 to be especially efficient in trimming peptides bound onto MHCI. We find no evidence for this however, because, in all cases tested, binding of a peptide onto MHCI protected it from ERAP1 activity. Furthermore, ERAP2 and the unrelated aminopeptidase LAP appear to be just as efficient in trimming a 12-mer peptide (AI12) in preformed complexes with B08. This finding suggests that the apparent trimming of AI12 is rather due to the properties of the B08/AI12 complex rather than the aminopeptidase used. In fact, fast dissociation of AI12 and subsequent solution trimming is the simplest possible model that can account for these observations. Furthermore, specialization for trimming of peptides bound onto MHC would necessitate some sort of interaction between ERAP1 and MHCI. Whereas this interaction could be expected to be transient due to the nature of the enzymatic reaction, it should be stabilized using transition-state analogue substrates as demonstrated previously (40, 49). However, our analysis failed to demonstrate the existence of a ternary ERAP1/peptide/MHCI complex, whereas the binary ERAP1-peptide and MHCI-peptide complexes could be detected. This finding suggests that ERAP1 cannot directly access the N terminus of a 12-mer peptide that is bound onto MHCI, at least under the experimental conditions tested here.

A recent study demonstrated ERAP1-mediated peptide trimming of a 16-mer peptide that was anchored onto the MHCI via a disulfide bond near its C terminus (23). In this case, ERAP1 trimming cannot possibly follow peptide full dissociation because the peptide is covalently bound onto the MHCI, but the peptide N terminus could transiently detach from the A-pocket and extend away from the MHCI as previously modeled (31). A long overhang could be structurally consistent with ERAP1 trimming, but steric hindrance and lack of activation by the regulatory site should make trimming less efficient. Indeed, in a recent study, the authors had to use a 100-fold higher concentration of ERAP1 to achieve similar trimming of the peptide-MHCI compared with the peptide in solution (37). Therefore, even in that case, MHCI binding protected, rather than promoted, peptide trimming.

As with any *in vitro* study, our study's conclusions are limited to the components of the *in vitro* system used. In particular, given that inside the cell, MHCI loading is facilitated by the PLC, it is conceivable that the PLC could facilitate, or even mediate, an ERAP1-MHCI interaction that could drive on-MHCI trimming in cells (57). Such an interaction, however, has not been demonstrated yet, and structural analysis of the PLC has suggested that it is topologically unlikely (29). Accordingly, and despite our efforts, we were unable to demonstrate any molecular interaction between cell-purified PLC and ERAP1 or ERAP2, even when using a N-terminally extended antigenic peptide that carried a transition state analogue N terminus optimized to have high affinity for ERAP1. This result is in accordance with the rest of our observations that suggest that antigenic peptide precursor trimming by ERAP1 takes place in

solution, without the peptide having any significant and/or stable interactions with the MHCI-binding groove.

In summary, we performed a thorough comparison of peptide trimming by ERAP1, in solution and in preformed complexes with MHCI. We find that solution trimming is always faster than for preformed MHCI-peptide complexes and that in all cases, MHCI binding protects the peptide from ERAP1 trimming. Furthermore, we demonstrate that when apparent on-MHC trimming is observed, it is limited by the peptide's dissociation kinetics, and we could find no evidence for any ERAP1-MHCI interaction, even within the context of native PLC. Thus, we propose that ERAP1-mediated antigenic peptide processing, even when demonstrated using preformed MHCI-peptide complexes, can be fully explained by well-established properties of components of the system: 1) the ability of ERAP1 to trim peptides in solution and 2) the dynamic binding of peptides onto MHCI (58). We conclude that with current evidence, there is no reason to adopt more auxiliary trimming modes that involve on-MHCI trimming and that the well-established solution trimming is sufficient to explain experimental observations (26).

Experimental procedures

*HLA-B*08:01 and β_2-microglobulin expression and purification*

Both the HLA-B*08:01 heavy chain and β_2-microglobulin were expressed as inclusion bodies in *Escherichia coli* BL21 DE3 cells, induced at A_{600} of 0.8 with 1 mM isopropyl-1-thio-D-galactopyranoside (AppliChem, A4773). Cells were harvested after 4 h by centrifugation (4,000 × *g*, 15 °C, 15 min). Cells were disrupted both by enzymatic lysis with lysozyme (AppliChem, A3711, 1 mg/ml suspension) and osmotic shock by sucrose (BDH Laboratory Supplies) solution (25% (w/v) sucrose, 50 mM Tris-HCl, pH 8, 1 mM EDTA (PanReac Quimica, A5097) and 0.1% (w/v) NaN_3 (Sigma–Aldrich, S2002)) and deoxycholic acid (Thermo Fisher Scientific, BP349100) solution (1% (w/v) deoxycholic acid, 1% (v/v) Triton X-100 (Thermo Fisher Scientific, BP151-100), 20 mM Tris-HCl, pH 8, 100 mM NaCl (AppliChem, A2942), and 0.1% (w/v) NaN_3). DNase (Sigma–Aldrich, DN25) and $MgCl_2$ (Sigma–Aldrich, M2670) were added at a final concentration of 10 μg/ml suspension and 5 mM, respectively. The pellet was then subjected to three subsequent washes (after each wash pellet was centrifuged at 8,000 × *g*, 4 °C, 20 min) with Triton X-100 solution (0.5% (w/v) Triton X-100, 50 mM Tris-HCl, pH 8, 100 mM NaCl, 1 mM EDTA, and 0.1% (w/v) NaN_3) followed by three subsequent washes with Tris-HCl (Tris Ultrapure from AppliChem (A1086), hydrochloric acid from AppliChem (AL1021)) solution (50 mM Tris-HCl, pH 8, 1 mM EDTA, and 0.1% (w/v) NaN_3). Finally, inclusion bodies were solubilized using urea (Applichem, A8113) solution (8 M urea, 25 mM MES (Sigma–Aldrich, M3671), pH 6, and 10 mM EDTA) and stored at −80 °C until needed.

*HLA-A*02:01 expression and purification*

HLA-A*02 heavy chain was expressed as inclusion bodies in *E. coli* strain XL-1 Blue cells without induction. A single colony from LB agar Petri dishes (agar molecular biology grade from AppliChem (A3477)) was inoculated at 2 ml of Luria-Bertani broth (1% (w/v) Tryptone BioChemica from AppliChem (A1553), 0.5% (w/v) yeast extract for molecular biology from AppliChem (A3732), 0.5% NaCl, 1% glucose from PanReac Quimica (A3666)) containing 100 μg/ml ampicillin for 8 h at 37 °C. Afterward, cell culture was transferred to a flask containing 200 ml of LB broth and 100 μg/ml ampicillin (AppliChem, A0839). Incubation followed for 20 h at 37 °C. Subsequently, cells were harvested by centrifugation (4,000 × *g*, 15 °C, 15 min). Purification was conducted by the same procedure that was followed for HLA-B*08:01 heavy chain and β_2-microglobulin.

*Expression and purification of HLA-B*58:01*

HLA-B*5801 was expressed in BL21(DE3) cells harboring the HLA-B*5801/pET22b(+) expression plasmid (33). *E. coli* cells at 0.6–0.8 A_{600}, were induced with 1 mM isopropyl-1-thio-D-galactopyranoside for 4 h at 37 °C for the expression of HLA-B*5801 inclusion bodies. Cells were harvested at 4000 rpm after induction and were resuspended in the extraction buffer (50 mM Tris-HCl, 100 mM NaCl, 10 mM $MgCl_2$, 1% Triton X-100, pH 8.2) with freshly added lysozyme (2 mg/ml), DNase, and PMSF (1 mM). Cells in extraction buffer were sonicated, and inclusion bodies were collected at 8000 rpm for 30 min. Inclusion bodies were again resuspended in the same buffer, and the above step is repeated to efficiently lyse cells and for a pure preparation of inclusion bodies. The inclusion bodies were washed three times with wash buffer (50 mM Tris, 20 mM EDTA, pH 8.0) to remove detergent and other soluble proteins. Purified inclusion bodies were resuspended in 8 M urea and stored at −80 °C.

Expression and purification of ERAP1 and ERAP2

High-five (Hi5) insect cells were grown in Sf-900II culture medium (Thermo Fisher Scientific, 12658019) at 27 °C. Infection with recombinant baculovirus was carried out in 50-ml flasks at a cell density of 1–1.5 × 10^6 cells/ml, and incubation was continued by gentle shaking at 27 °C for 72 h. The culture medium was centrifuged (4500 × *g*, 15 min, 4 °C), and the supernatant was dialyzed overnight against buffer containing 10 mM NaH_2PO_4 (Sigma–Aldrich, 04269) adjusted to pH 8 with NaOH (Merck, S8045) and 100 mM NaCl. Supernatant was then equilibrated to binding buffer (50 mM NaH_2PO_4, pH 8, 300 mM NaCl, and 10 mM imidazole). Batch binding onto nickel-nitrilotriacetic acid–agarose beads (Thermo Fisher Scientific, R90101) was achieved by mild rotation at 4 °C for 2 h. Supernatant and beads were afterward loaded to a nickel-nitrilotriacetic acid column and washed several times with buffer: 50 mM NaH_2PO_4, pH 8, 300 mM NaCl, and 10–30 mM imidazole (AppliChem, A3635). Elution was performed by 50 mM NaH_2PO_4, pH 8, 300 mM NaCl, and 150 mM imidazole. Final dialysis of elution fractions was conducted overnight against 10 mM Hepes (Sigma–Aldrich, 54457), pH 7, and 100 mM NaCl. Protein aliquots were kept at −80 °C after the addition of 10% (v/v) glycerol (Sigma–Aldrich, G5516).

Purification of peptide-loading complex from Raji cells

The peptide-loading complex was purified from Raji cells with all of its components (TAP1/2, ERp57, calreticulin, tapasin, and HLA-A*03) utilizing the *herpesvirus* I TAP inhibitor

ICP47 equipped with an SBP tag (ICP47-SBP) as described previously (29).

Peptide-loading complex pulldown assay

Purified PLC was bound on high-capacity streptavidin-agarose beads (Pierce) after purification from Raji cells and incubated for 30 min at 4 °C on an overhead rotor with a 4-fold excess of either DG057, ERAP1, ERAP2, or a mixture of ERAP1/ERAP2. In addition, ERAP1, ERAP2, or ERAP1/ERAP2 mixture was incubated for 30 min with equimolar ratios of DG057 before incubation with the PLC for 30 min at 4 °C on an overhead rotor. The supernatant was collected, and the beads were washed three times with buffer (20 mM Hepes, pH 7.5, 150 mM NaCl, 0.02% glyco-diosgenin, 1.25 mM benzamidine, 0.5 mM PMSF). The PLC was eluted by boiling in 5× SDS-PAGE loading buffer. Protein pulldown was analyzed by SDS-PAGE (4–12% BisTris gels, NuPAGE™, stained by InstantBlue™).

Peptide-loading complex size-exclusion analysis

3.5 pmol of purified PLC were incubated with ERAP1, ERAP2, or ERAP1/2 mixtures in the presence or absence of DG057 as described above for 30 min at 4 °C, respectively. SEC analysis was performed with a Shimadzu HPLC system equipped with a Shodex KW404-4F column in running buffer (20 mM Hepes, pH 7.5, 150 mM NaCl, 0.01% glyco-diosgenin).

*Folding of HLA-B*58:01*

HLA-B*58:01 (56 mg), β_2-microglobulin (28 mg), and dipeptide GF (200 mg) was diluted in 100 mM Tris-HCl, pH 8.0, 0.4 M arginine, 0.5 mM oxidized GSH, 1.5 mM reduced GSH, 2 mM EDTA, 4 M urea, 0.2 mM PMSF, 1× protease inhibitor mixture in a volume of 500 ml and kept at 4 °C for 2 h on stirring. After 2 h, peptide was added (TW10 or its variants) (3 μM), and the mixture was left at 4 °C for 24 h while stirring. The folding solution was then dialyzed for 4 h against 0.1 M urea, 10 mM Tris-HCl, pH 8.0, and for another 40 h against 10 mM Tris-HCl, pH 8.0, at 4 °C. After dialysis, the folding mixture was filtered and concentrated for purification on a Superdex 200 gel filtration column preequilibrated in PBS.

*Folding of HLA-B*08:01 and HLA-A*02:01*

Protein complexes were folded *in vitro* from urea-solubilized inclusion bodies of heavy chain (1 μM) and β_2-microglobulin (2 μM) in the presence of peptide (GeneCust and JPT Peptide Technologies) in excess (40 μM). Peptides were dissolved in DMSO (MP Biomedicals, MFCD00002089). The complexes were reconstituted in folding buffer that contained 0.4 M arginine (AppliChem, A3675), 100 mM Tris-HCl, pH 8, 2 mM EDTA, 5% (v/v) glycerol, 5 mM reduced GSH (AppliChem, A2084), 0.5 mM L-GSH oxidized (Acros Organics, 320220050), and 0.1 mM PMSF (AppliChem, A0999). Complexes were purified by size-exclusion chromatography in a Sephacryl S-200 high-resolution column using buffer containing 150 mM NaCl and 10 mM Tris-HCl, pH 8. Purified complexes were concentrated to 8–12 μM and kept at −80 °C after the addition of 10% (v/v) glycerol.

DSF

DSF was performed in the LightCycler 96 RT-PCR instrument (Roche Applied Science). Reaction mixtures (total volume 20 μl) consisted of 16 μl of protein complex (final concentration 8 μM) and 4 μl of 50× SYPRO Orange (Sigma–Aldrich, S5692) dye (stock solution of 5000× was diluted in 10 mM Tris-HCl, pH 8, 150 mM NaCl). Excitation wavelength was set at 533 nm and emission wavelength at 572 nm. A temperature gradient from 25 to 80 °C at a rate of 0.02 °C/s was used to generate the denaturation curves. The denaturation curves were plotted as fluorescence intensity *versus* temperature, and first-derivative curves were generated using the LightCycler 96 1.1 software. The minimum point of the first derivative of each curve provided the T_m.

Thermal stability evaluation by CD

CD spectra were acquired using a Jasco J-715 instrument equipped with a PTC-348 temperature control unit. Temperature was increased from 20 to 90 °C at 1 °C/min, and data points were acquired every 0.2 °C by monitoring a wavelength of 230 nm. The assay was performed using 120 μl of protein complex at 8–10 μM. Data were fitted to a sigmoidal Boltzmann equation using GraphPad Prism.

Peptide dissociation followed by SYPRO Orange

The assay was performed in the LightCycler 96 RT-PCR instrument. Reaction mixtures (total volume 20 μl) consisted of 16 μl of protein complex (final concentration 8 μM) and 4 μl of 50× SYPRO Orange dye. Excitation wavelength was set at 533 nm and emission at 572 nm. The temperature was set at 37 °C for the duration of the experiment. Data were fit to a one-phase decay model using GraphPad Prism. For HLA-B*58 complexes, DSF was performed on Bio-Rad C1000 thermal cycler RT-PCR under the FRET channel. The reaction mix contained 10 μM HLA-B58-peptide complexes and 10× (v/v) SYPRO Orange (Invitrogen) in a 20-μl volume in PBS in 96-well plates. For thermal stability measurements, the temperature scan rate was 1 °C/min, and the temperature range scanned was 20–95 °C. For calculating T_m values, relative fluorescence units values obtained for different complexes at different temperatures were normalized to calculate the percentage of protein folded or unfolded, and normalized values were fit to cumulative-Gaussian percentages. For more detailed analysis, the temperature derivative of the melting curve was computed and was plotted. The data were plotted on GraphPad Prism 7. For kinetic measurements, 10 μM B58 complexes were incubated with 10× SYPRO Orange with fluorescence measured after every 5 min. The data were fit to a one-phase exponential function to calculate the half-lives of class I MHC.

Kinetic competition assays followed by native PAGE

HLA-B*0801 complexes with 12-mer peptides LL12 and AI12 were incubated with a 10-fold higher concentration (100 μM) of the high-affinity peptide ALRSRYWAI at 37 °C (total reaction volume 50 μl). After incubation, samples were immediately subjected to native-PAGE analysis. HLA-B*0801 complexes with 12-mer peptides LL12 and AI12 were also incu-

bated with either ERAP1 or ERAP2 at various concentrations (2–100 nM). After incubation, samples were collected, 100 μM L-leucinethiol (Sigma–Aldrich, L8397) was added, and samples were immediately subjected to native-PAGE analysis.

Peptide trimming followed by HPLC

TW10 peptide variants (11–25-mers, 10 μM) or HLA-B*58 folded with N-extended peptides (10 μM) were incubated with ERAP1 (20 or 100 nM) at room temperature in 20 mM Tris-HCl, pH 7.5, 100 mM NaCl. The reactions at different time points (0–120 min) were terminated by adding 0.1% (v/v) TFA. Quenched reaction mixtures were analyzed on C18-RP-HPLC using an acetonitrile gradient (20–40%) in 0.05% (v/v) TFA. The percentage of the substrate peptide left after hydrolysis was calculated by integration of the area under each peptide peak. Data were plotted on GraphPad Prism 7.

Peptide-trimming assay followed by MALDI TOF-MS

Peptides or MHCI-peptide complexes were diluted to 10 μM in buffer containing 10 mM Tris-HCl, pH 8, 150 mM NaCl. Total reaction volume was 50 μl. Aminopeptidases (ERAP1, ERAP2, or LAP) were added at various final concentrations (from 2 to 100 nM), and the mixtures were incubated at 37 °C. Reactions were quenched by adding TFA (AppliChem, A0697) to a 1% final concentration and stored at −80 °C until ready to analyze. For analysis, samples were diluted 1:10 with matrix solution (7 mg/ml α-cyano-4-hydroxycinnamic acid in 50% acetonitrile (AppliChem, 131881), 0.1% TFA) and spotted on a stainless steel MALDI target using the dried droplet method. Peptide masses were determined by MALDI-TOF/TOF MS (Ultraflex TOF/TOF, Bruker Daltonics, Bremen, Germany), a peak list was created with Flexanalysis version 3.3 software (Bruker), smoothing was applied with the Savitzky–Golay algorithm (width 0.2 *m/z*, cycle number 1), and a signal/noise threshold ratio of 2.5 was allowed. 10 × 1000 shots/spectrum were acquired at a laser frequency of 500 Hz. The instrument was operated in reflector mode with matrix suspension set to 600 *m/z*. Spectra were acquired in positive ion mode in the range of 750–3500 *m/z*. All spectra and respective peak lists were exported with Flexanalysis version 3.3.

Fluorigenic enzymatic assay

Measurements were performed using a Spark 10M (TECAN) multimode microplate reader. The fluorescent substrate leucine-aminomethylcoumarin (Sigma–Aldrich, L2145) was used for ERAP1, and LAP (Sigma–Aldrich, L5006) and arginine-aminomethylcoumarin (Sigma–Aldrich, A2027) were used for ERAP2. Excitation was adjusted at 380 nm and emission at 460 nm. The reaction was performed in 50 mM Hepes, pH 7, 100 mM NaCl with 100 μM substrate in a total volume of 150 μl. Enzyme final concentration was 10 nM for ERAP1, 2 nM for ERAP2, and 3 nM for LAP. Increasing concentrations of DG078 phosphinic peptide (either in solution or in complex with HLA*B0801) were added at the start of the reaction. The IC_{50} of DG078 inhibitor was calculated by using the equation log (inhibitor) *versus* response-variable slope using GraphPad Prism.

Synthesis of pseudophosphinic peptides DG078 and DG057

Phosphinic peptide DG078 (H-AΨ(P(O)(OH)CH_2)KAA-LRSRYWAI-OH) and DG057 (H-hFΨ(P(O)(OH)CH_2)GGS-GSGSQFGGGSQY-OH) were prepared by applying standard solid-phase peptide synthesis on trityl alcohol lanterns (15 μmol/pin) using an Fmoc chemical protocol (Fig. S17). Trityl alcohol lanterns were converted to the corresponding trityl chloride by using a solution of acetyl chloride in dry dichloromethane (1:10, v/v) at room temperature. For DG078, Fmoc-Ile-OH (30 μmol/pin), the first amino acid of the sequence, was attached on trityl chloride lanterns by using *N,N*-diisopropylethylamine (18 μl/pin) in dry dichloromethane (0.4 ml/pin) at room temperature for 12 h (59, 60). The loading amount of Fmoc-Ile-OH was estimated to be 13.6 μmol/pin, after removal with 0.5% TFA/dichloromethane (room temperature, 1 h) from the polymer support. In a similar manner, the first amino acid for the synthesis of DG057, Fmoc-Tyr(^{t}Bu)-OH, was coupled with a loading of 11.1 μmol/pin. In both peptides, Fmoc deprotection was achieved by soaking the lanterns into a solution of 20% piperidine in *N,N*-dimethylformamide over 1 h for each cycle of the synthesis. Fmoc-protected amino acids (45 μmol/pin) were coupled to the developing peptide by using 1-hydroxybenzotriazole (45 μmol/pin), and *N,N*-diisopropylcarbodiimide (45 μmol/pin) in dichloromethane/*N,N*-dimethylformamide (6:1) (0.4 ml/pin), and each coupling reaction was allowed to proceed for 5 h. For DG078, to avoid incomplete couplings during the introduction of the fifth and seventh amino acids (both Arg), *N,N*-dimethylformamide was replaced by *N*-methyl-2-pyrrolidone, and the mixture was sonicated at 50 °C for 3–4 h. No deviation from the standard protocol was necessary for the synthesis of DG057. Side-chain protected amino acids used were as follows: Fmoc-Tyr(^{t}Bu)-OH,, Fmoc-Gln(Trt)-OH, Fmoc-Ser(^{t}Bu)-OH, Fmoc-Trp(Boc)-OH, and Fmoc-Arg(Pbf)-OH. Coupling of the building block Boc-(*R*)-Ala(PO(OAd)-CH_2)-(*R,S*)-Lys(Boc)OH (23 μmol/pin) and Boc-(R)-hPhe(PO(OAd)-CH_2)-GlyOH (23 μmol/pin), for DG078 and DG057, respectively, was performed using the coupling conditions described above (36 μmol/pin of each reagent). Deprotection and removal of the final pseudopeptides from the polymer support was accomplished by using a solution of TFA/dichloromethane/triisopropylsilane/H_2O (39:58:2:1) for 3 h at room temperature. After concentration *in vacuo*, the crude products were precipitated in cold diethyl ether. DG078 and DG057 were obtained after purification by analytical reverse-phase HPLC and characterized by MS. DG078: electrospray-MS m/z (z = 1): calculated for $[C65H106N19O16P+H]^+$ 1439.78; found: 1440.79; DG057: electrospray-MS *m/z* (*z* = 1): calculated for $[C64H90N17O25P+H]^+$ 1528.6; found: 1528.5.

Synthesis of Boc-(R)-Ala(PO(OAd)-CH_2)-(R,S)-Lys(Boc)OH

For the synthesis of building block Boc-(*R*)-Ala(PO(OAd)-CH_2)-(*R,S*)-Lys(Boc)OH (**6**), 4-aminobutanol was subjected to Boc protection and subsequent Appel iodination, according to literature procedures, to afford iodide **2** in 54% yield for the two steps (61, 62) (Fig. S18). Iodide **2** (1.8 g, 6.0 mmol) was dissolved in 28 ml of a 1:1 mixture of *N,N*-dimethylformamide/toluene; $HC(CO_2Et)_3$ (1.53 g, 6.6 mmol), K_2CO_3 (1.08 g, 7.82 mmol) was

added; and the mixture was refluxed for 1 h, according to our previously published procedure (44). After aqueous workup, the crude product was saponified with KOH (10 eq) in EtOH, and the resulting diacid was subjected to Knoevenagel condensation, affording acrylic acid analogue of **3** (887 mg, 61% yield for three steps) (44). The resulting acid (787 mg, 3.23 mmol) was dissolved in CH_2Cl_2 (5 ml), and benzyl alcohol (350 mg, 3.24 mmol), *N*,*N*-dicyclohexylcarbodiimide (801 mg, 3.89 mmol), and 4-dimethylaminopyridine (40 mg, 0.32 mmol) were successively added. After stirring for 5 h at room temperature, the mixture was filtrated, and the filtrates were concentrated and dissolved in Et_2O (30 ml) and H_2O (10 ml), and the organic layer was washed with 1 M HCl (10 ml), 5% $NaHCO_3$ (10 ml), and brine (5 ml), dried over Na_2SO_4, and concentrated *in vacuo*. Compound **3** (895 mg, 83%) was obtained as colorless viscous oil after silica gel column chromatography (phosphatidylethanolamine 40–60 °C/ethyl acetate 9:1 → 2:1). ^{1}H NMR (200 MHz, $CDCl_3$) δ 1.42 (s, 9H), 1.41–1.53 (m, 4H), 2.24–2.38 (m, 2H), 3.01–3.15 (m, 2H), 4.51 (br s, 1H), 5.54 (q, J = 1.4 Hz, 1H), 6.15–6.21 (m, 1H), 7.23–7.39 (m, 5H); ^{13}C NMR (200 MHz, $CDCl_3$) δ 25.6, 28.4, 28.5, 29.6, 31.5, 40.5, 66.4, 79.2, 125.3, 128.1, 128.2, 128.6, 136.1, 140.3, 156.1, 167.0. In a mixture of aminophosphinic acid **4** (300 mg, 1.44 mmol) and **3** (574 mg, 1.72 mmol) in CH_2Cl_2, BSA (1.07 ml, 4.31 mmol) and TMSCl (0.55 ml, 4.31 mmol) were added under argon atmosphere at −78 °C, and the resulting mixture was stirred at room temperature for 5 days. Then the mixture was cooled at 0 °C, EtOH (1.5 ml) was slowly added, and stirring was continued for 20 min. After removal of the volatiles *in vacuo*, the residue was taken up by ethyl acetate (20 ml), and the organic solution was washed with 2 M HCl (2 × 10 ml) and brine (10 ml). The organic layer was dried over Na_2SO_4 and evaporated *in vacuo* to afford the crude product. Compound **5** (490 mg, 56%) was obtained as a gummy solid after silica gel column chromatography ($CHCl_3$/MeOH/AcOH 7:0.03:0:03 → 7:0.3:0.3). ^{1}H NMR (200 MHz, CD_3OD) δ 1.28 and 1.32 (2 × d, J = 14.5 Hz, 3H), 1.42 and 1.44 (2 × s, 18H), 1.41–2.02 (m, 7H), 2.07–2.37 (m, 1H), 2.74–3.05 (m, 3H), 3.78–4.00 (m, 1H), 5.08–5.24 (m, 2H), 7.17–7.54 (m, 5H); ^{13}C NMR (200 MHz, CD_3OD) δ 13.7, 13.9, 24.9, 25.0, 28.7, 28.8, 29.2, 29.4 (2 × d, J = 90 Hz), 34.5, 34.7, 34.9, 35.1, 40.3, 40.4, 41.0, 45.71, 46.52 (2 × d, J = 107 Hz), 67.59, 79.73, 80.71, 129.2, 129.4, 129.5, 137.4, 157.4 (d, J = 5.2 Hz), 158.3, 176.1 (d, J = 6.7 Hz); ^{31}P NMR (81 MHz, CD_3OD) δ 50.3, 50.7. For the preparation of **6**, application of our previously developed two-step protocol on intermediate **5** (90 mg, 0.17 mmol) involving adamantylation of phosphinic acid moiety and subsequent removal of benzyl group by hydrogenolysis led to 90 mg of target building block **6** (93%, yield for two steps) as a mixture of four diastereoisomers. ^{31}P NMR (81 MHz, CD_3OD) δ 51.9, 52.1, 52.4, 52.6; HRMS (*m*/*z*): $[M + H]^+$ calcd. for $C_{29}H_{52}N_2O_8P^+$, 587.3456 found, 587.3460.

Molecular dynamics simulations

The four HLA-B8–peptide complexes used for the MD study were based on the X-ray crystal structure of HLA-B*08:01 complex with the influenza A virus nucleoprotein epitope **E**LRSRYWA**I** (PDB code 5WMQ) (42). Side-chain atoms in residues with alternative conformation B were removed, and protonation states of histidine residues were estimated using the H++ server at the experimental pH value of 6.5, ionic strength of 0.15 M, and default dielectric constants (63). The second system, HLA-B*08:01 in complex with **A**LRSRYWA**I** (HLA-B08/AI9), was produced from the X-ray–based model by removing the side-chain atoms except for C^β of the Glu(P1) residue of EI9. Modeling of the extended 12-mer peptides **A**RAALRSRYWA**I** (AI12) and **L**SILLKHKKAA**L** (LL12) was based on the hypothesis that the peptides would bulge out to favorably accommodate their N and C termini within the binding groove of HLA-B08. First, we prepared the model of AI12 using MODELLER version 9.21 and the crystallographic coordinates of residues P1 (E) and P4–P9 (SRYWAI) as template, so as to constrain the position of the N terminus inside pocket A of the HLA-B08. From 100 models that were generated, the peptide-binding groove of HLA-B08 (residues 1–180) with bound AI12 were subjected to unrestraint energy minimization using AMBER version 16 and the ff14SB force field in implicit solvent (generalized Born OBC model gb-5) (64, 65). The lowest-potential energy structures were visually investigated to select five low-energy conformations of AI12 with the highest pairwise root mean square deviation (RMSD), to sample the configurational space of the HLA-B08/AI12 more efficiently from different starting structures (Fig. S7). For the modeling of HLA-B08/LL12, we used the selected five models of AI12 as template, with the aim to compare their conformational space with initial conditions as similar as possible (Fig. S8).

Molecular dynamics simulations were performed using the GPU-accelerated PMEMD module of AMBER version 16 (66). All systems were immersed in truncated octahedral pre-equilibrated water boxes (TIP3P) with a buffer distance of 12 Å around the solute atoms. Sodium ions were added to neutralize the total charge of the systems, and ff14SB parameters were applied using the LEaP module of AMBER (67). The equilibration method of 10 ns and simulation parameters were as described (68). After a 1-ns equilibration of the systems at 300 K under isothermal-isobaric ensemble (NPT) conditions, production runs of 500 ns were performed in the canonical ensemble (NVT). Specifically, five sets of MDs for each B08/EI9 and B08/AI9 complex were seeded with random initial velocities (Fig. S9) and one run for each of the five initial models with variable peptide conformation for B08/AI12 and B08/LL12 (Fig. S10), for an aggregate simulation time of 2.5 μs for each system. Snapshots of the B08-peptide complexes were kept every 10 ps, and trajectory analysis was carried out using the CPPTRAJ module of AMBER (69). The atomic root mean square fluctuations of the C^α atoms of the peptides were calculated after RMSD fitting of the C^α atoms of the antigen-binding groove (residues 1–180) of the HLA-B08 heavy chain (Fig. S11). Considering the effect of the initial conformation selected for each of the 12-mer peptides to the results of their fluctuations at the timescale of the MDs, we performed five additional 500-ns simulations for each B08/AI12 and B08/LL12 complex, both initiated using the same conformation that was employed in simulations labeled "sim-2" (Figs. S9–S11). This conformation displayed the lowest RMSD and RMSF values for both peptides during the MDs, but in particular for the more labile AI12. The results of the peptide C^α RMSF values for each of the five sets of

simulations seeded with different initial velocity distributions (labeled as "sim2a-2e"; Fig. S13 (*A* and *B*)) further supported our observation that A12 is considerably more labile than LL12, irrespective of the initial conformation employed in the MDs (Figs. S12 and S13 (*C* and *D*)). Trajectory visualization and rendering of the figures was performed using VMD version 1.9 (70).

Data availability statement

All data described are available in the article and associated supporting information. Numerical values used for generation of graphs are available upon request to the corresponding author (Efstratios Stratikos, E-mail: stratos@rrp.demokritos.gr).

Author contributions—G. M., R. A., A. D., J. Z., M. M., A. V., R. T., A. P., and E. S. data curation; G. M., R. A., A. D., J. Z., M. M., A. V., A. M., A. L., D. G., R. T., A. P., and L. J. S. investigation; G. M., R. A., A. D., J. Z., M. M., A. V., A. M., A. L., D. G., R. T., A. P., and E. S. methodology; G. M., A. D., R. T., A. P., L. J. S., and E. S. writing-review and editing; R. T., A. P., L. J. S., and E. S. conceptualization; R. T., A. P., L. J. S., and E. S. supervision; R. T., L. J. S., and E. S. funding acquisition; A.P. formal analysis; E. S. writing-original draft.

*Acknowledgments—We thank Jia-Huai Wang (Dana-Farber Cancer Institute, Harvard Medical School) for providing HLA-B*5801 expression plasmid, Brian M. Baker (University of Notre Dame) for providing the HLA-A*02:01 expression plasmid, and Marlene Bouvier (University of Illinois at Chicago) for providing the HLA-B*08 expression plasmid. We thank Dr. Simon Trowitzsch (Goethe University Frankfurt) for helpful discussions.*

References

1. Rock, K. L., Reits, E., and Neefjes, J. (2016) Present yourself! By MHC class I and MHC class II molecules. *Trends Immunol.* **37,** 724–737 CrossRef Medline
2. Weimershaus, M., Evnouchidou, I., Saveanu, L., and van Endert, P. (2013) Peptidases trimming MHC class I ligands. *Curr. Opin. Immunol.* **25,** 90–96 CrossRef Medline
3. York, I. A., Chang, S. C., Saric, T., Keys, J. A., Favreau, J. M., Goldberg, A. L., and Rock, K. L. (2002) The ER aminopeptidase ERAP1 enhances or limits antigen presentation by trimming epitopes to 8–9 residues. *Nat. Immunol.* **3,** 1177–1184 CrossRef Medline
4. Serwold, T., Gonzalez, F., Kim, J., Jacob, R., and Shastri, N. (2002) ERAAP customizes peptides for MHC class I molecules in the endoplasmic reticulum. *Nature* **419,** 480–483 CrossRef Medline
5. York, I. A., Brehm, M. A., Zendzian, S., Towne, C. F., and Rock, K. L. (2006) Endoplasmic reticulum aminopeptidase 1 (ERAP1) trims MHC class I-presented peptides *in vivo* and plays an important role in immunodominance. *Proc. Natl. Acad. Sci. U.S.A.* **103,** 9202–9207 CrossRef Medline
6. Hammer, G. E., Gonzalez, F., James, E., Nolla, H., and Shastri, N. (2007) In the absence of aminopeptidase ERAAP, MHC class I molecules present many unstable and highly immunogenic peptides. *Nat. Immunol.* **8,** 101–108 CrossRef Medline
7. James, E., Bailey, I., Sugiyarto, G., and Elliott, T. (2013) Induction of protective antitumor immunity through attenuation of ERAAP function. *J. Immunol.* **190,** 5839–5846 CrossRef Medline
8. Cifaldi, L., Romania, P., Falco, M., Lorenzi, S., Meazza, R., Petrini, S., Andreani, M., Pende, D., Locatelli, F., and Fruci, D. (2015) ERAP1 regulates natural killer cell function by controlling the engagement of inhibitory receptors. *Cancer Res.* **75,** 824–834 CrossRef Medline
9. Stratikos, E. (2014) Regulating adaptive immune responses using small molecule modulators of aminopeptidases that process antigenic peptides. *Curr. Opin. Chem. Biol.* **23,** 1–7 CrossRef Medline
10. López de Castro, J. A., Alvarez-Navarro, C., Brito, A., Guasp, P., Martín-Esteban, A., and Sanz-Bravo, A. (2016) Molecular and pathogenic effects of endoplasmic reticulum aminopeptidases ERAP1 and ERAP2 in MHC-I-associated inflammatory disorders: towards a unifying view. *Mol. Immunol.* **77,** 193–204 CrossRef Medline
11. Stratikos, E., Stamogiannos, A., Zervoudi, E., and Fruci, D. (2014) A role for naturally occurring alleles of endoplasmic reticulum aminopeptidases in tumor immunity and cancer pre-disposition. *Front. Oncol.* **4,** 363 CrossRef Medline
12. Cortes, A., Pulit, S. L., Leo, P. J., Pointon, J. J., Robinson, P. C., Weisman, M. H., Ward, M., Gensler, L. S., Zhou, X., Garchon, H. J., Chiocchia, G., Nossent, J., Lie, B. A., Førre, Ø., Tuomilehto, J., *et al.* (2015) Major histocompatibility complex associations of ankylosing spondylitis are complex and involve further epistasis with ERAP1. *Nat. Commun.* **6,** 7146 CrossRef Medline
13. de Castro, J. A. L. (2018) How ERAP1 and ERAP2 shape the peptidomes of disease-associated MHC-I proteins. *Front. Immunol.* **9,** 2463 CrossRef Medline
14. Nagarajan, N. A., de Verteuil, D. A., Sriranganadane, D., Yahyaoui, W., Thibault, P., Perreault, C., and Shastri, N. (2016) ERAAP shapes the peptidome associated with classical and nonclassical MHC class I molecules. *J. Immunol.* **197,** 1035–1043 CrossRef Medline
15. Barnea, E., Melamed Kadosh, D., Haimovich, Y., Satumtira, N., Dorris, M. L., Nguyen, M. T., Hammer, R. E., Tran, T. M., Colbert, R. A., Taurog, J. D., and Admon, A. (2017) The human leukocyte antigen (HLA)-B27 peptidome *in vivo*, in spondyloarthritis-susceptible HLA-B27 transgenic rats and the effect of Erap1 deletion. *Mol. Cell. Proteomics* **16,** 642–662 CrossRef Medline
16. Alvarez-Navarro, C., Martín-Esteban, A., Barnea, E., Admon, A., and López de Castro, J. A. (2015) Endoplasmic reticulum aminopeptidase 1 (ERAP1) polymorphism relevant to inflammatory disease shapes the peptidome of the birdshot chorioretinopathy-associated HLA-A*29:02 antigen. *Mol. Cell. Proteomics* **14,** 1770–1780 CrossRef Medline
17. Martín-Esteban, A., Sanz-Bravo, A., Guasp, P., Barnea, E., Admon, A., and López de Castro, J. A. (2017) Separate effects of the ankylosing spondylitis associated ERAP1 and ERAP2 aminopeptidases determine the influence of their combined phenotype on the HLA-B*27 peptidome. *J. Autoimmun.* **79,** 28–38 CrossRef Medline
18. Evnouchidou, I., Momburg, F., Papakyriakou, A., Chroni, A., Leondiadis, L., Chang, S. C., Goldberg, A. L., and Stratikos, E. (2008) The internal sequence of the peptide-substrate determines its N-terminus trimming by ERAP1. *PLoS ONE* **3,** e3658 CrossRef Medline
19. Nguyen, T. T., Chang, S. C., Evnouchidou, I., York, I. A., Zikos, C., Rock, K. L., Goldberg, A. L., Stratikos, E., and Stern, L. J. (2011) Structural basis for antigenic peptide precursor processing by the endoplasmic reticulum aminopeptidase ERAP1. *Nat. Struct. Mol. Biol.* **18,** 604–613 CrossRef Medline
20. Stamogiannos, A., Koumantou, D., Papakyriakou, A., and Stratikos, E. (2015) Effects of polymorphic variation on the mechanism of endoplasmic reticulum aminopeptidase 1. *Mol. Immunol.* **67,** 426–435 CrossRef Medline
21. Chang, S. C., Momburg, F., Bhutani, N., and Goldberg, A. L. (2005) The ER aminopeptidase, ERAP1, trims precursors to lengths of MHC class I peptides by a "molecular ruler" mechanism. *Proc. Natl. Acad. Sci. U.S.A.* **102,** 17107–17112 CrossRef Medline
22. Ombrello, M. J., Kastner, D. L., and Remmers, E. F. (2015) Endoplasmic reticulum-associated amino-peptidase 1 and rheumatic disease: genetics. *Curr. Opin. Rheumatol.* **27,** 349–356 CrossRef Medline
23. Chen, H., Li, L., Weimershaus, M., Evnouchidou, I., van Endert, P., and Bouvier, M. (2016) ERAP1-ERAP2 dimers trim MHC I-bound precursor peptides; implications for understanding peptide editing. *Sci. Rep.* **6,** 28902 CrossRef Medline
24. Reeves, E., Edwards, C. J., Elliott, T., and James, E. (2013) Naturally occurring ERAP1 haplotypes encode functionally distinct alleles with fine substrate specificity. *J. Immunol.* **191,** 35–43 CrossRef Medline
25. Kanaseki, T., Blanchard, N., Hammer, G. E., Gonzalez, F., and Shastri, N. (2006) ERAAP synergizes with MHC class I molecules to make the final

cut in the antigenic peptide precursors in the endoplasmic reticulum. *Immunity* **25,** 795–806 CrossRef Medline
26. Mpakali, A., Maben, Z., Stern, L. J., and Stratikos, E. (2019) Molecular pathways for antigenic peptide generation by ER aminopeptidase 1. *Mol. Immunol.* **113,** 50–57 CrossRef Medline
27. Papakyriakou, A., and Stratikos, E. (2017) The role of conformational dynamics in antigen trimming by intracellular aminopeptidases. *Front. Immunol.* **8,** 946 CrossRef Medline
28. Trowitzsch, S., and Tampe, R. (2020) Multifunctional chaperone and quality control complexes in adaptive immunity. *Annu. Rev. Biophys.* CrossRef Medline
29. Blees, A., Januliene, D., Hofmann, T., Koller, N., Schmidt, C., Trowitzsch, S., Moeller, A., and Tampé, R. (2017) Structure of the human MHC-I peptide-loading complex. *Nature* **551,** 525–528 CrossRef Medline
30. Infantes, S., Samino, Y., Lorente, E., Jiménez, M., García, R., Del Val, M., and López, D. (2010) Cutting edge: H-2L(d) class I molecule protects an HIV N-extended epitope from *in vitro* trimming by endoplasmic reticulum aminopeptidase associated with antigen processing. *J. Immunol.* **184,** 3351–3355 CrossRef Medline
31. Papakyriakou, A., Reeves, E., Beton, M., Mikolajek, H., Douglas, L., Cooper, G., Elliott, T., Werner, J. M., and James, E. (2018) The partial dissociation of MHC class I-bound peptides exposes their N terminus to trimming by endoplasmic reticulum aminopeptidase 1. *J. Biol. Chem.* **293,** 7538–7548 CrossRef Medline
32. Sette, A., Vitiello, A., Reherman, B., Fowler, P., Nayersina, R., Kast, W. M., Melief, C. J., Oseroff, C., Yuan, L., Ruppert, J., Sidney, J., del Guercio, M. F., Southwood, S., Kubo, R. T., Chesnut, R. W., *et al.* (1994) The relationship between class I binding affinity and immunogenicity of potential cytotoxic T cell epitopes. *J. Immunol.* **153,** 5586–5592 Medline
33. Li, X., Lamothe, P. A., Walker, B. D., and Wang, J. H. (2017) Crystal structure of HLA-B*5801 with a TW10 HIV Gag epitope reveals a novel mode of peptide presentation. *Cell Mol. Immunol.* **14,** 631–634 CrossRef Medline
34. Tynan, F. E., Burrows, S. R., Buckle, A. M., Clements, C. S., Borg, N. A., Miles, J. J., Beddoe, T., Whisstock, J. C., Wilce, M. C., Silins, S. L., Burrows, J. M., Kjer-Nielsen, L., Kostenko, L., Purcell, A. W., McCluskey, J., and Rossjohn, J. (2005) T cell receptor recognition of a "super-bulged" major histocompatibility complex class I-bound peptide. *Nat. Immunol.* **6,** 1114–1122 CrossRef Medline
35. Hassan, C., Chabrol, E., Jahn, L., Kester, M. G., de Ru, A. H., Drijfhout, J. W., Rossjohn, J., Falkenburg, J. H., Heemskerk, M. H., Gras, S., and van Veelen, P. A. (2015) Naturally processed non-canonical HLA-A*02:01 presented peptides. *J. Biol. Chem.* **290,** 2593–2603 CrossRef Medline
36. Remesh, S. G., Andreatta, M., Ying, G., Kaever, T., Nielsen, M., McMurtrey, C., Hildebrand, W., Peters, B., and Zajonc, D. M. (2017) Unconventional peptide presentation by major histocompatibility complex (MHC) class I allele HLA-A*02:01: breaking confinement. *J. Biol. Chem.* **292,** 5262–5270 CrossRef Medline
37. Li, L., Batliwala, M., and Bouvier, M. (2019) ERAP1 enzyme-mediated trimming and structural analyses of MHC I-bound precursor peptides yield novel insights into antigen processing and presentation. *J. Biol. Chem.* **294,** 18534–18544 CrossRef Medline
38. de Castro, J. A. L., and Stratikos, E. (2019) Intracellular antigen processing by ERAP2: molecular mechanism and roles in health and disease. *Hum. Immunol.* **80,** 310–317 CrossRef Medline
39. Towne, C. F., York, I. A., Neijssen, J., Karow, M. L., Murphy, A. J., Valenzuela, D. M., Yancopoulos, G. D., Neefjes, J. J., and Rock, K. L. (2005) Leucine aminopeptidase is not essential for trimming peptides in the cytosol or generating epitopes for MHC class I antigen presentation. *J. Immunol.* **175,** 6605–6614 CrossRef Medline
40. Mpakali, A., Giastas, P., Mathioudakis, N., Mavridis, I. M., Saridakis, E., and Stratikos, E. (2015) Structural basis for antigenic peptide recognition and processing by endoplasmic reticulum (ER) aminopeptidase 2. *J. Biol. Chem.* **290,** 26021–26032 CrossRef Medline
41. Hellman, L. M., Yin, L., Wang, Y., Blevins, S. J., Riley, T. P., Belden, O. S., Spear, T. T., Nishimura, M. I., Stern, L. J., and Baker, B. M. (2016) Differential scanning fluorimetry based assessments of the thermal and kinetic stability of peptide-MHC complexes. *J. Immunol. Methods* **432,** 95–101 CrossRef Medline
42. Rowntree, L. C., Nguyen, T. H. O., Halim, H., Purcell, A. W., Rossjohn, J., Gras, S., Kotsimbos, T. C., and Mifsud, N. A. (2018) Inability to detect cross-reactive memory T cells challenges the frequency of heterologous immunity among common viruses. *J. Immunol.* **200,** 3993–4003 CrossRef Medline
43. Giastas, P., Neu, M., Rowland, P., and Stratikos, E. (2019) High-resolution crystal structure of endoplasmic reticulum aminopeptidase 1 with bound phosphinic transition-state analogue inhibitor. *ACS Med. Chem. Lett.* **10,** 708–713 CrossRef Medline
44. Kokkala, P., Mpakali, A., Mauvais, F. X., Papakyriakou, A., Daskalaki, I., Petropoulou, I., Kavvalou, S., Papathanasopoulou, M., Agrotis, S., Fonsou, T. M., van Endert, P., Stratikos, E., and Georgiadis, D. (2016) Optimization and structure-activity relationships of phosphinic pseudotripeptide inhibitors of aminopeptidases that generate antigenic peptides. *J. Med. Chem.* **59,** 9107–9123 CrossRef Medline
45. Thomas, C., and Tampé, R. (2019) MHC I chaperone complexes shaping immunity. *Curr. Opin. Immunol.* **58,** 9–15 CrossRef Medline
46. Stratikos, E. (2014) Modulating antigen processing for cancer immunotherapy. *Oncoimmunology* **3,** e27568 CrossRef Medline
47. Koumantou, D., Barnea, E., Martin-Esteban, A., Maben, Z., Papakyriakou, A., Mpakali, A., Kokkala, P., Pratsinis, H., Georgiadis, D., Stern, L. J., Admon, A., and Stratikos, E. (2019) Editing the immunopeptidome of melanoma cells using a potent inhibitor of endoplasmic reticulum aminopeptidase 1 (ERAP1). *Cancer Immunol. Immunother.* **68,** 1245–1261 CrossRef Medline
48. Sui, L., Gandhi, A., and Guo, H. C. (2016) Crystal structure of a polypeptide's C-terminus in complex with the regulatory domain of ER aminopeptidase 1. *Mol. Immunol.* **80,** 41–49 CrossRef Medline
49. Giastas, P., Mpakali, A., Papakyriakou, A., Lelis, A., Kokkala, P., Neu, M., Rowland, P., Liddle, J., Georgiadis, D., and Stratikos, E. (2019) Mechanism for antigenic peptide selection by endoplasmic reticulum aminopeptidase 1. *Proc. Natl. Acad. Sci. U.S.A.* **116,** 26709–26716 CrossRef Medline
50. Pymm, P., Illing, P. T., Ramarathinam, S. H., O'Connor, G. M., Hughes, V. A., Hitchen, C., Price, D. A., Ho, B. K., McVicar, D. W., Brooks, A. G., Purcell, A. W., Rossjohn, J., and Vivian, J. P. (2017) MHC-I peptides get out of the groove and enable a novel mechanism of HIV-1 escape. *Nat. Struct. Mol. Biol.* **24,** 387–394 CrossRef Medline
51. Sanchez-Ruiz, J. M. (1992) Theoretical analysis of Lumry-Eyring models in differential scanning calorimetry. *Biophys. J.* **61,** 921–935 CrossRef Medline
52. Komov, L., Kadosh, D. M., Barnea, E., Milner, E., Hendler, A., and Admon, A. (2018) Cell surface MHC class I expression is limited by the availability of peptide-receptive "empty" molecules rather than by the supply of peptide ligands. *Proteomics* **18,** e1700248 CrossRef Medline
53. Admon, A. (2019) ERAP1 shapes just part of the immunopeptidome. *Hum. Immunol.* **80,** 296–301 CrossRef Medline
54. Blanchard, N., and Shastri, N. (2008) Coping with loss of perfection in the MHC class I peptide repertoire. *Curr. Opin. Immunol.* **20,** 82–88 CrossRef Medline
55. Hearn, A., York, I. A., and Rock, K. L. (2009) The specificity of trimming of MHC class I-presented peptides in the endoplasmic reticulum. *J. Immunol.* **183,** 5526–5536 CrossRef Medline
56. Zervoudi, E., Papakyriakou, A., Georgiadou, D., Evnouchidou, I., Gajda, A., Poreba, M., Salvesen, G. S., Drag, M., Hattori, A., Swevers, L., Vourloumis, D., and Stratikos, E. (2011) Probing the S1 specificity pocket of the aminopeptidases that generate antigenic peptides. *Biochem. J.* **435,** 411–420 CrossRef Medline
57. Hulpke, S., and Tampé, R. (2013) The MHC I loading complex: a multitasking machinery in adaptive immunity. *Trends Biochem. Sci.* **38,** 412–420 CrossRef Medline
58. Wieczorek, M., Abualrous, E. T., Sticht, J., Álvaro-Benito, M., Stolzenberg, S., Noé, F., and Freund, C. (2017) Major histocompatibility*Front. Immunol.* **8,** 292 CrossRef Medline

59. Rasoul, F., Ercole, F., Pham, Y., Bui, C. T., Wu, Z., James, S. N., Trainor, R. W., Wickham, G., and Maeji, N. J. (2000) Grafted supports in solid-phase synthesis. *Biopolymers* **55,** 207–216 CrossRef Medline
60. Doi, T., Numajiri, Y., Takahashi, T., Takagi, M., and Shin-ya, K. (2011) Solid-phase total synthesis of (−)-apratoxin A and its analogues and their biological evaluation. *Chem. Asian J.* **6,** 180–188 CrossRef Medline
61. Zhu, H., Wickenden, J. G., Campbell, N. E., Leung, J. C., Johnson, K. M., and Sammis, G. M. (2009) Construction of carbo- and heterocycles using radical relay cyclizations initiated by alkoxy radicals. *Org. Lett.* **11,** 2019–2022 CrossRef Medline
62. Boddy, A. J., Affron, D. P., Cordier, C. J., Rivers, E. L., Spivey, A. C., and Bull, J. A. (2019) Rapid assembly of saturated nitrogen heterocycles in one-pot: diazo-heterocycle "stitching" by N-H insertion and cyclization. *Angew. Chem. Int. Ed. Engl.* **58,** 1458–1462 CrossRef Medline
63. Anandakrishnan, R., Aguilar, B., and Onufriev, A. V. (2012) H++ 3.0: automating pK prediction and the preparation of biomolecular structures for atomistic molecular modeling and simulations. *Nucleic Acids Res.* **40,** W537–W541 CrossRef Medline
64. Maier, J. A., Martinez, C., Kasavajhala, K., Wickstrom, L., Hauser, K. E., and Simmerling, C. (2015) ff14SB: improving the accuracy of protein side chain and backbone parameters from ff99SB. *J. Chem. Theory Comput.* **11,** 3696–3713 CrossRef Medline
65. Onufriev, A., Bashford, D., and Case, D. A. (2004) Exploring protein native states and large-scale conformational changes with a modified generalized Born model. *Proteins* **55,** 383–394 CrossRef Medline
66. Salomon-Ferrer, R., Götz, A. W., Poole, D., Le Grand, S., and Walker, R. C. (2013) Routine microsecond molecular dynamics simulations with AMBER on GPUs. 2. Explicit solvent particle mesh Ewald. *J. Chem. Theory Comput.* **9,** 3878–3888 CrossRef Medline
67. Case, D. A., Cheatham, T. E., 3rd, Darden, T., Gohlke, H., Luo, R., Merz, K. M., Jr., Onufriev, A., Simmerling, C., Wang, B., and Woods, R. J. (2005) The Amber biomolecular simulation programs. *J. Comput. Chem.* **26,** 1668–1688 CrossRef Medline
68. Stamogiannos, A., Maben, Z., Papakyriakou, A., Mpakali, A., Kokkala, P., Georgiadis, D., Stern, L. J., and Stratikos, E. (2017) Critical role of interdomain interactions in the conformational change and catalytic mechanism of endoplasmic reticulum aminopeptidase 1. *Biochemistry* **56,** 1546–1558 CrossRef Medline
69. Roe, D. R., and Cheatham, T. E., 3rd. (2013) PTRAJ and CPPTRAJ: software for processing and analysis of molecular dynamics trajectory data. *J. Chem. Theory Comput.* **9,** 3084–3095 CrossRef Medline
70. Humphrey, W., Dalke, A., and Schulten, K. (1996) VMD: visual molecular dynamics. *J. Mol. Graph.* **14,** 33–38, 27–28 CrossRef Medline
71. Zarutskie, J. A., Sato, A. K., Rushe, M. M., Chan, I. C., Lomakin, A., Benedek, G. B., and Stern, L. J. (1999) A conformational change in the human major histocompatibility complex protein HLA-DR1 induced by peptide binding. *Biochemistry* **38,** 5878–5887 CrossRef Medline

A systematic re-examination of processing of MHCI-bound antigenic peptide precursors by endoplasmic reticulum aminopeptidase 1

George Mavridis, Richa Arya, Alexander Domnick, Jerome Zoidakis, Manousos Makridakis, Antonia Vlahou, Anastasia Mpakali, Angelos Lelis, Dimitris Georgiadis, Robert Tampé, Athanasios Papakyriakou, Lawrence J. Stern and Efstratios Stratikos

J. Biol. Chem. 2020, 295:7193-7210.
doi: 10.1074/jbc.RA120.012976 originally published online March 17, 2020

SUPPORTING DATA

A systematic re-examination of processing of MHCI-bound antigenic peptide precursors by ER aminopeptidase 1

George Mavridis[1], Richa Arya[4], Alexander Domnick[5], Jerome Zoidakis[2], Manousos Makridakis[2], Antonia Vlahou[2], Anastasia Mpakali[1], Angelos Lelis[3], Dimitris Georgiadis[3], Robert Tampé[5], Athanasios Papakyriakou[1], Lawrence J. Stern[4] and Efstratios Stratikos[1,*]

[1] National Centre for Scientific Research Demokritos, Agia Paraskevi, Greece
[2] Centre of Basic Research, Biomedical Research Foundation of the Academy of Athens, Athens, Greece
[3] Laboratory of Organic Chemistry, Chemistry Department, University of Athens, Athens, Greece
[4] University of Massachusetts Medical School, Worcester, MA, USA
[5] Institute of Biochemistry, Biocenter, Goethe University Frankfurt, Max-von-Laue-Str. 9, D-60438 Frankfurt/Main, Germany

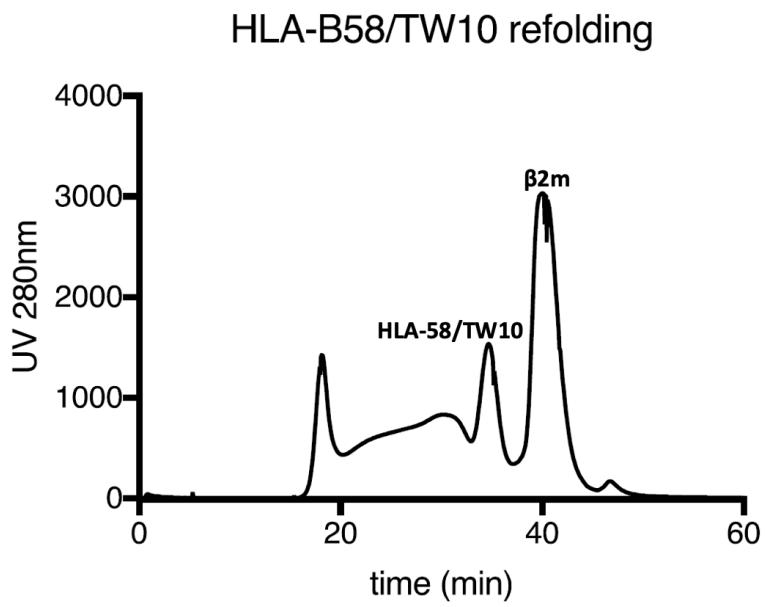

Supporting Figure 1: Folding of peptide TW10 with HLA-B*58. Chromatogram depicting elution of HLA-B*58 folded in the presence of peptide TW10 from a S200 size-exclusion column.

Peptide (length)	Sequence
TW10	TSTLQEQIGW
L-TW10 (11)	Leu-TSTLQEQIGW
L-AW13 (14)	Leu-AGTTSTLQEQIGW
L-DW15 (16)	Leu-DIAGTTSTLQEQIGW
L-RW18 (19)	Leu-RGSDIAGTTSTLQEQIGW
L-MW22 (23)	Leu-MGSGGSGGSGGSTSTLQEQIGW
L-GW24 (25)	Leu-GQGGSGGSGGSGGSTSTLQEQIGW

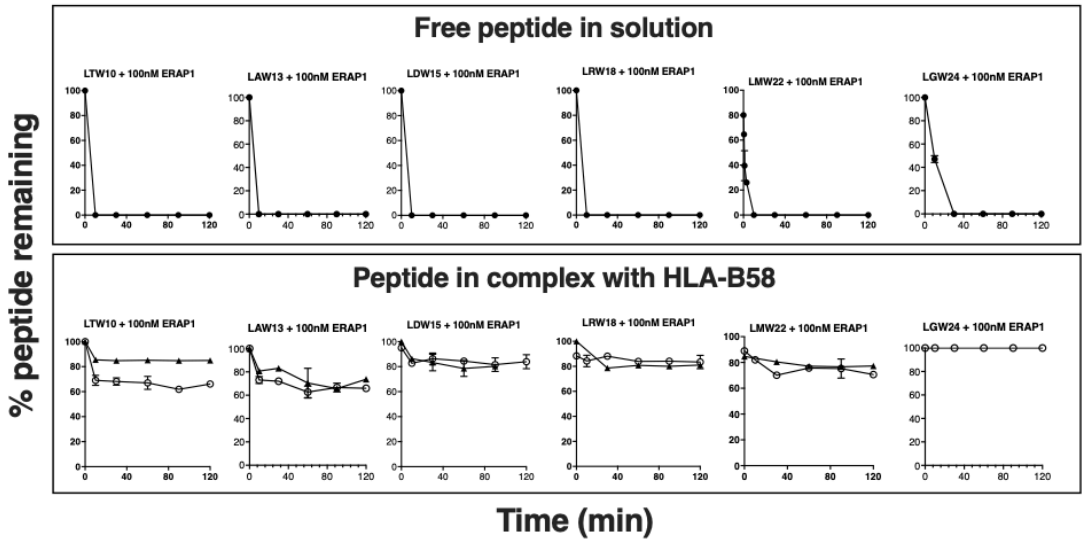

Supporting Figure 2: Trimming of peptides in solution and in pre-formed complexes with HLA-B58 by 100 nM ERAP1. Top, list of peptides used. Bottom, percent remaining peptide after incubation calculated by HPLC analysis. Filled circles correspond to peptide in solution, and empty circles and filled triangles to peptide in pre-formed complex with HLA-B58 (two replicates).

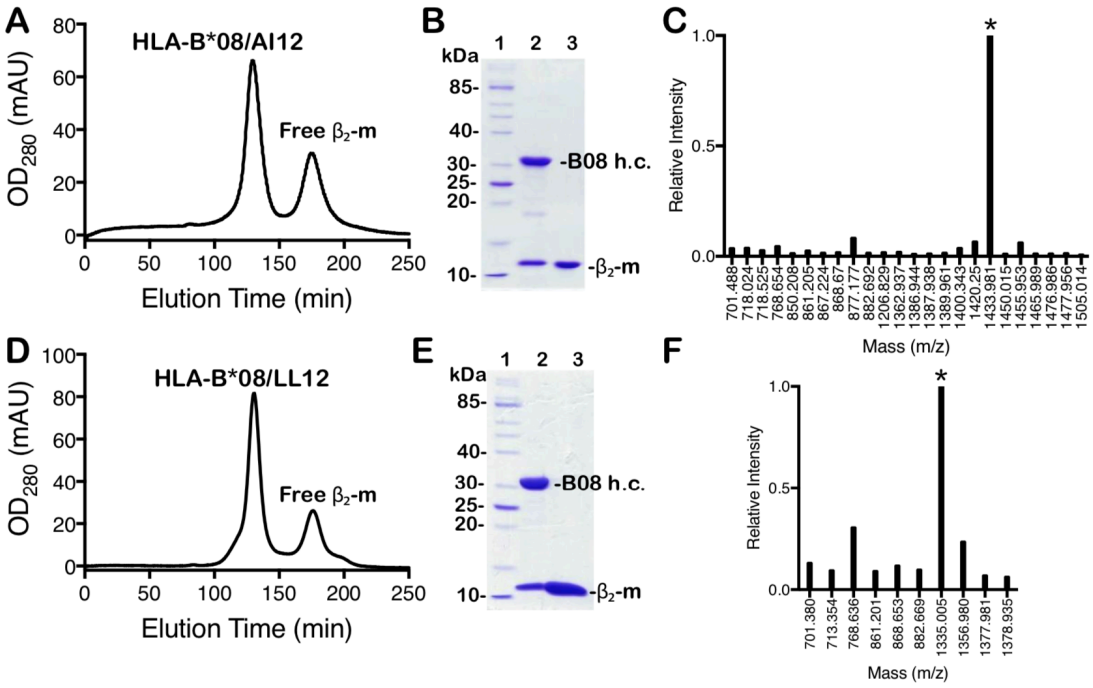

Supporting Figure 3: Folding peptide AI12 and LL12 with HLA-B*08. *Left,* chromatograms depicting elution of HLA-B*08 folded *in vitro* in the presence of peptides AI12 and LL12 respectively. *Middle,* SDS-PAGE analysis of the two major peaks of chromatogram. *Right,* MALDI-MS analysis of folded complex, indicating the mass of the bound peptide.

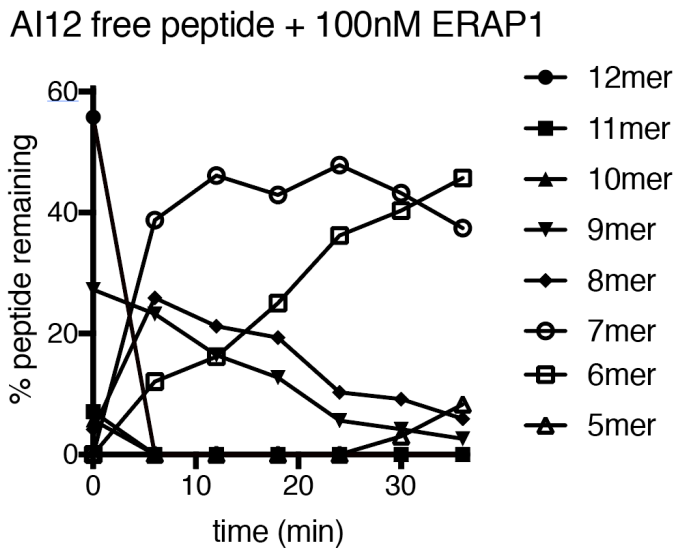

Supporting Figure 4: Trimming of AI12 in pre-formed complexes with HLA-B08 by ERAP1 followed by MALDI-MS.

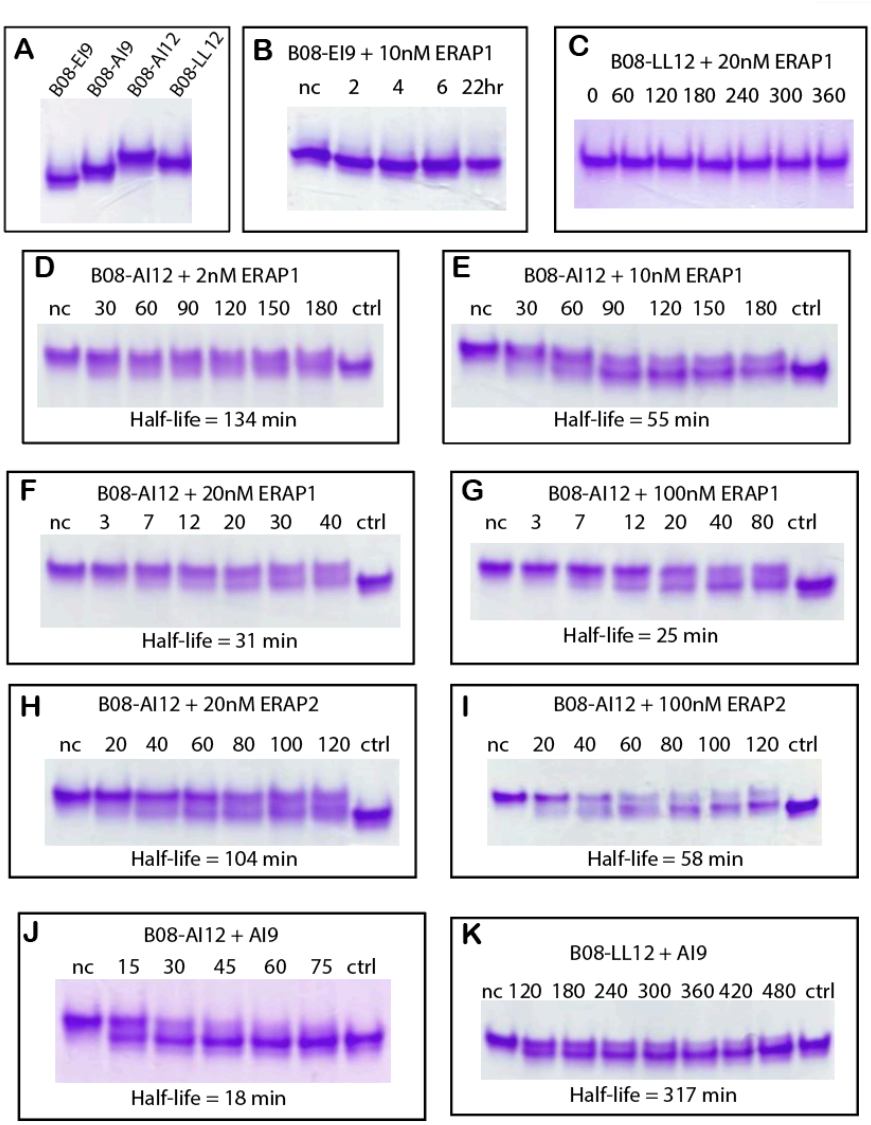

Supporting Figure 5: Panel A, changes in mobility in native-PAGE of HLA-B08 depending on loaded peptide. Panels B-I, changes in native-PAGE mobility of HLA-B08 loaded with indicated peptides, upon incubation with indicated concentration of ERAP1 or ERAP2. Calculated half-life of the initial complex is shown beneath every gel. Panels J-K, changes in native-PAGE mobility of HLA-B08 complexes with AI12 or LL12 upon incubation with excess epitope AI9. Gels in panels C, F and J are also shown in Figure 4 of the paper.

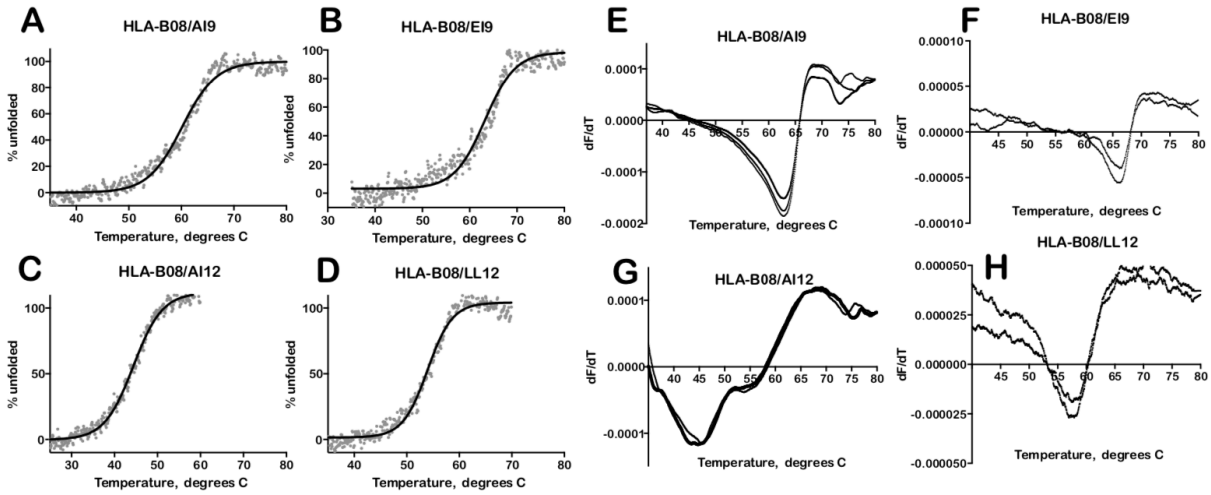

Supporting Figure 6: Panels A-D, circular dichroism melting curves of HLA-B*08 complexes. Panels E-H, first derivatives of melting curves of HLA-B*08 complexes followed by Differential Scanning Fluorimetry.

Supporting Table 1: Thermal stability of HLA-B08 complexes

HLA-B08 complex	T_m DSF (°C)
B08-AI12	47.8 ± 2.3
B08-LL12	57.7 ± 0.4
B08-ELRSRYWAI	66.1 ± 0.3
B08-ALRSRYWAI	63.6 ± 0.8

HLA-B08 complex	T_m by C.D. (°C)
B08-AI12	43.5 ± 0.2
B08-LL12	53.2 ± 0.2
B08-ELRSRYWAI	62.9 ± 0.2
B08-ALRSRYWAI	60.2 ± 0.2

Supporting Table 2: Kinetic stability of HLA-B08 complexes

HLA B08 complex	Half-life (min)
B08-AI12	9 ± 1
B08-LL12	362 ± 91
B08-EI9	891 ± 91
B08-Ai9	1056 ± 152
B08-DG078	12.7 ± 0.2

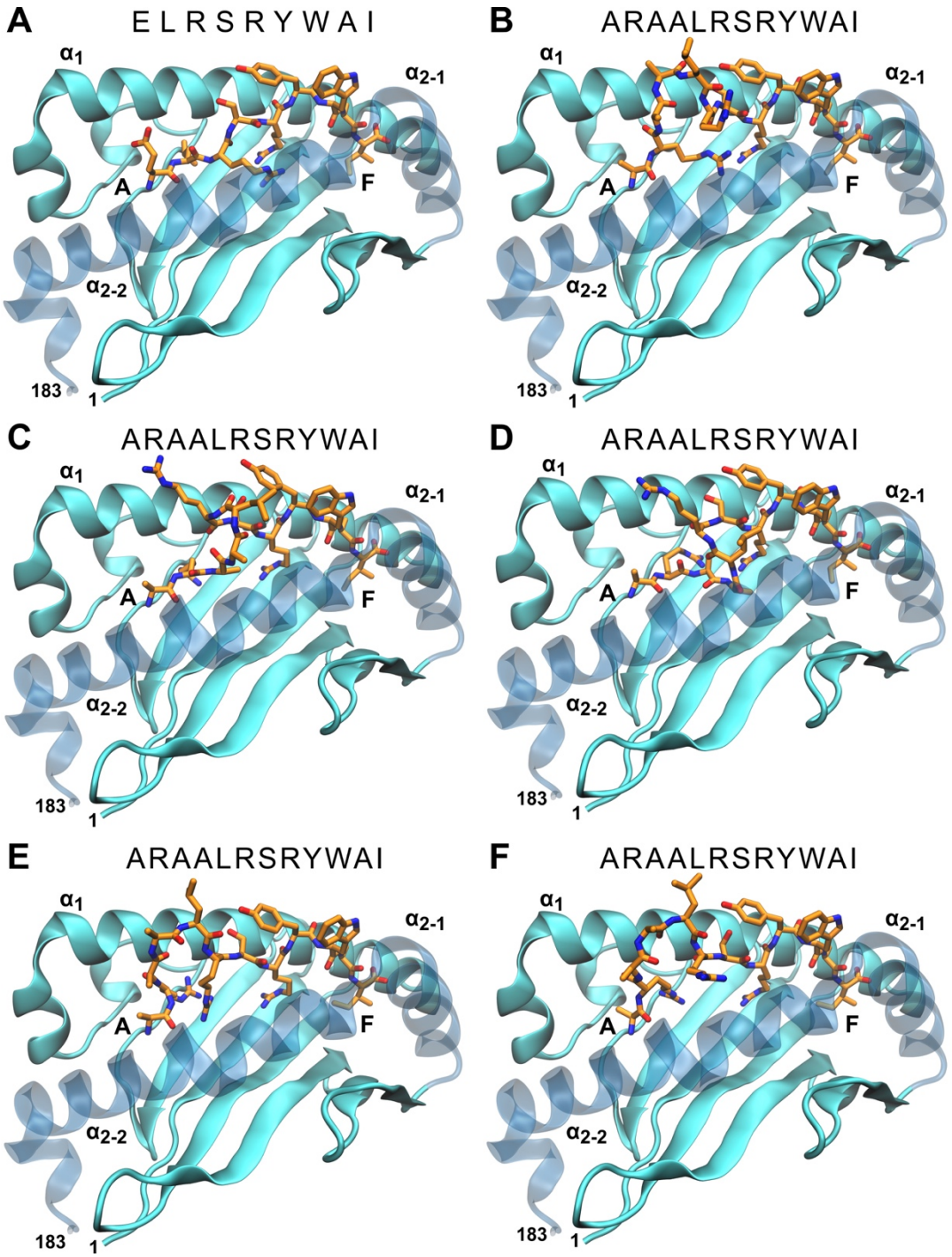

Supporting Figure 7. Ribbon representation of the antigen-binding groove of HLA-B08 (residues 1–183) illustrating the initial conformation of the peptide that was selected for the MD simulations. **(A)** HLA-B08/EI9 from the X-ray crystal structure, **(B-F)** the five different conformations of AI12 that were modelled on the basis of P1 and P4–P9 residues of EI9 as template. Helix α_2 is shown transparent and the N and C peptide termini binding pockets A and F, respectively, are indicated.

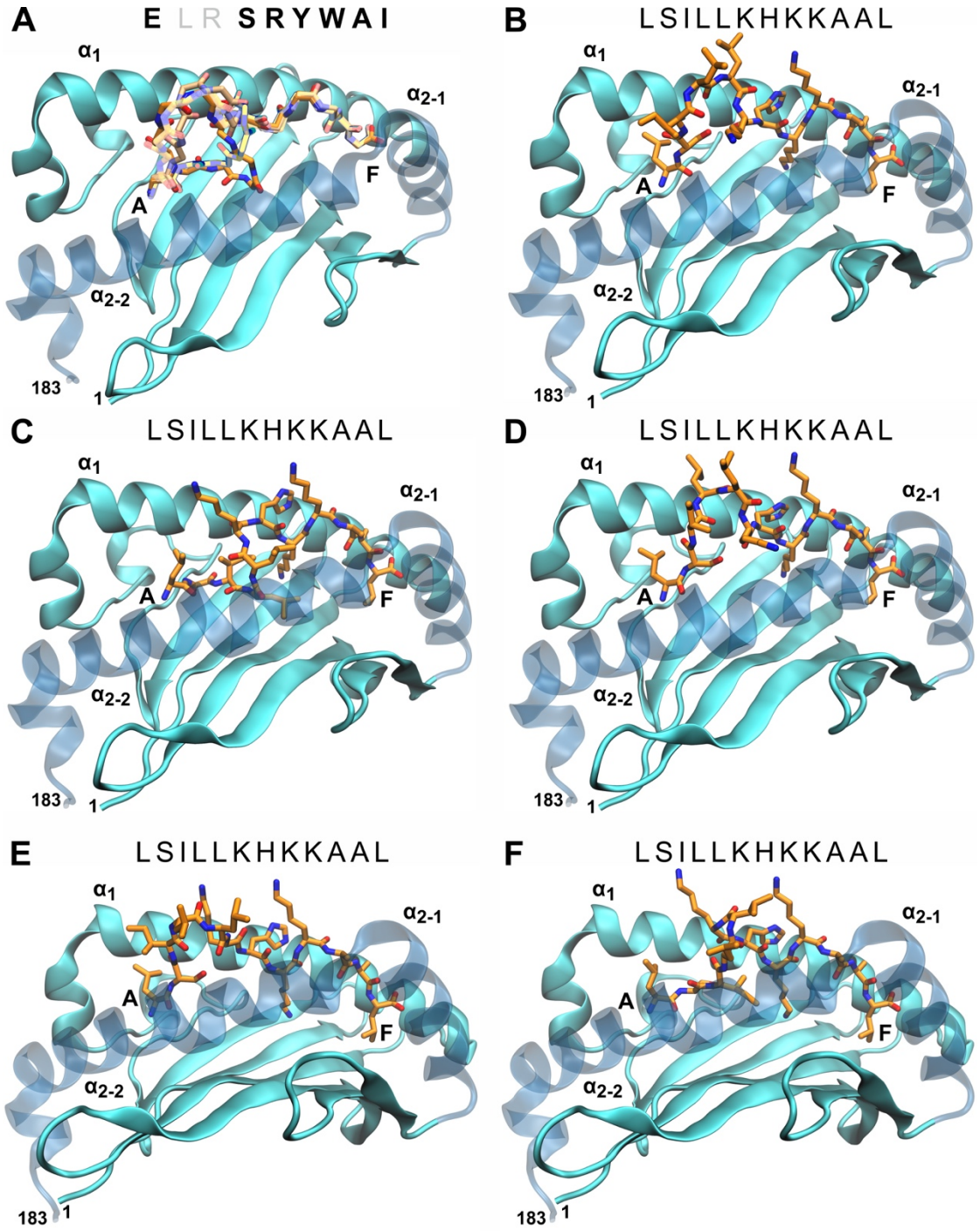

Supporting Figure 8. Ribbon representation of the antigen-binding groove of HLA-B08 (residues 1–183) illustrating the initial conformations of the 12mer peptide LL12 that were used for the MD simulations. **(A)** Backbone atoms of the peptide conformations from AI12 models that were used as templates for the modeling of LL12, **(B-F)** the 5 resulting models of LL12 in the peptide binding groove of HLA-B08. Helix α_2 is shown transparent and the N and C peptide termini binding pockets A and F, respectively, are indicated.

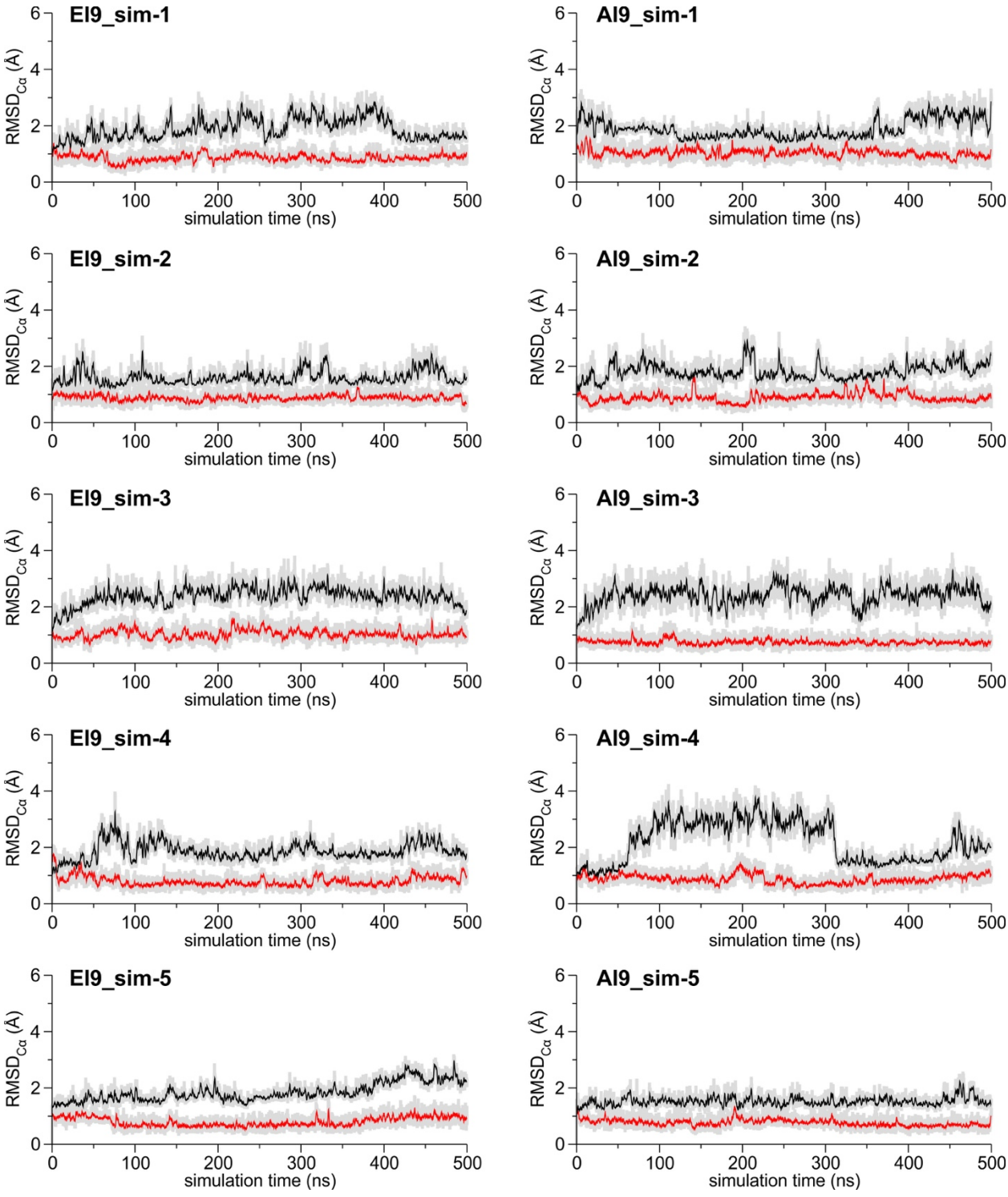

Supporting Figure 9. Plots of RMSDs of C_α atoms from the initial structure as a function of simulation time for the HLA-B08 antigen-binding domain (black lines) and for the 9mer peptides EI9 or AI9 (red lines), as indicated for each of the five replicate MD simulations. Straight lines are running averages over 100 steps (1 ns time) and the axes are in the same scale for comparison.

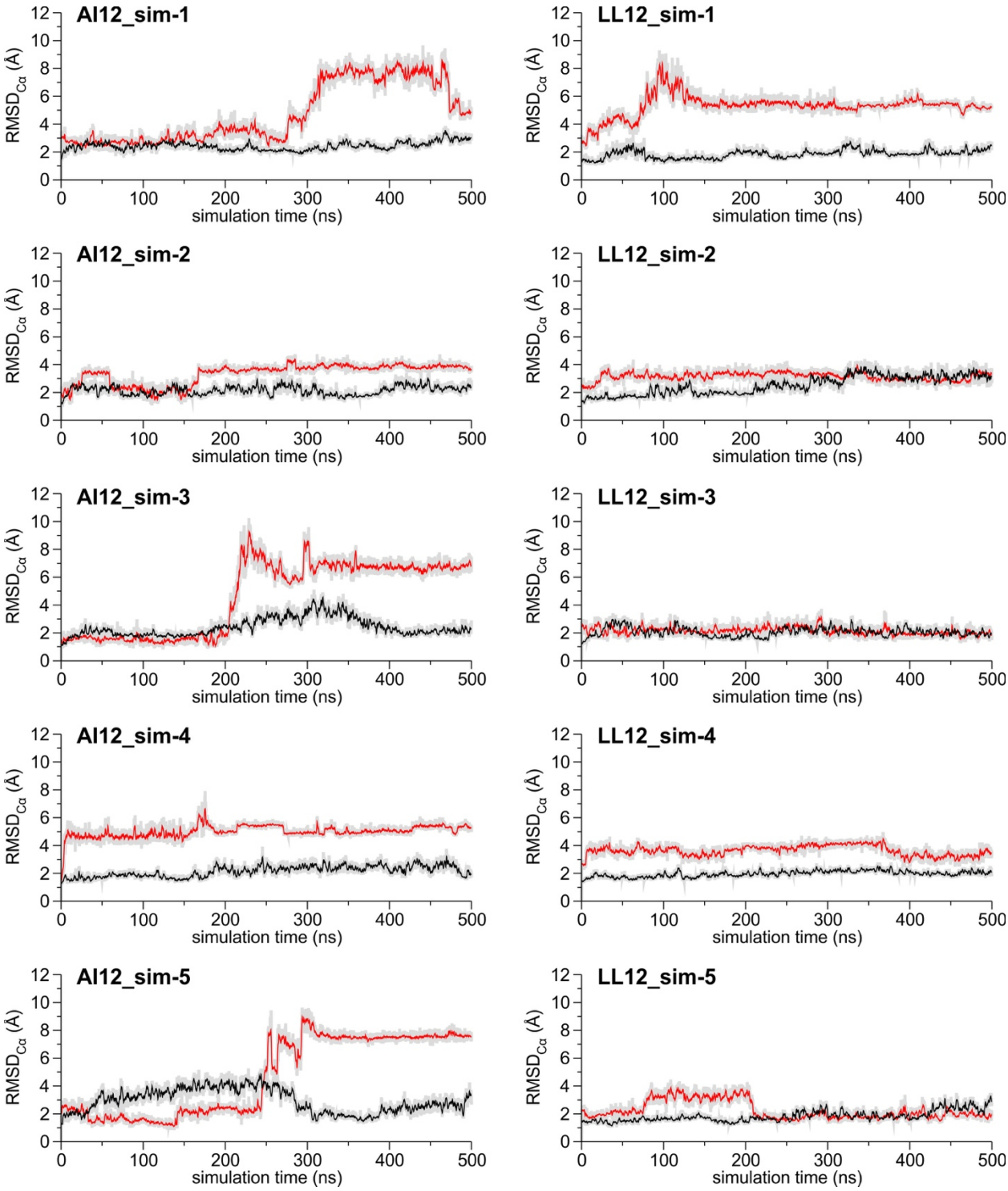

Supporting Figure 10. Plots of RMSDs of C_α atoms from the initial structure as a function of simulation time for the HLA-B08 antigen-binding domain (black lines) and for the 12mer peptides AI12 or LL12 (red lines), as indicated for each of the five MD simulations that were initiated with different peptide conformation (Supporting Figures 8, 9). Straight lines are running averages over 100 steps (1 ns time).

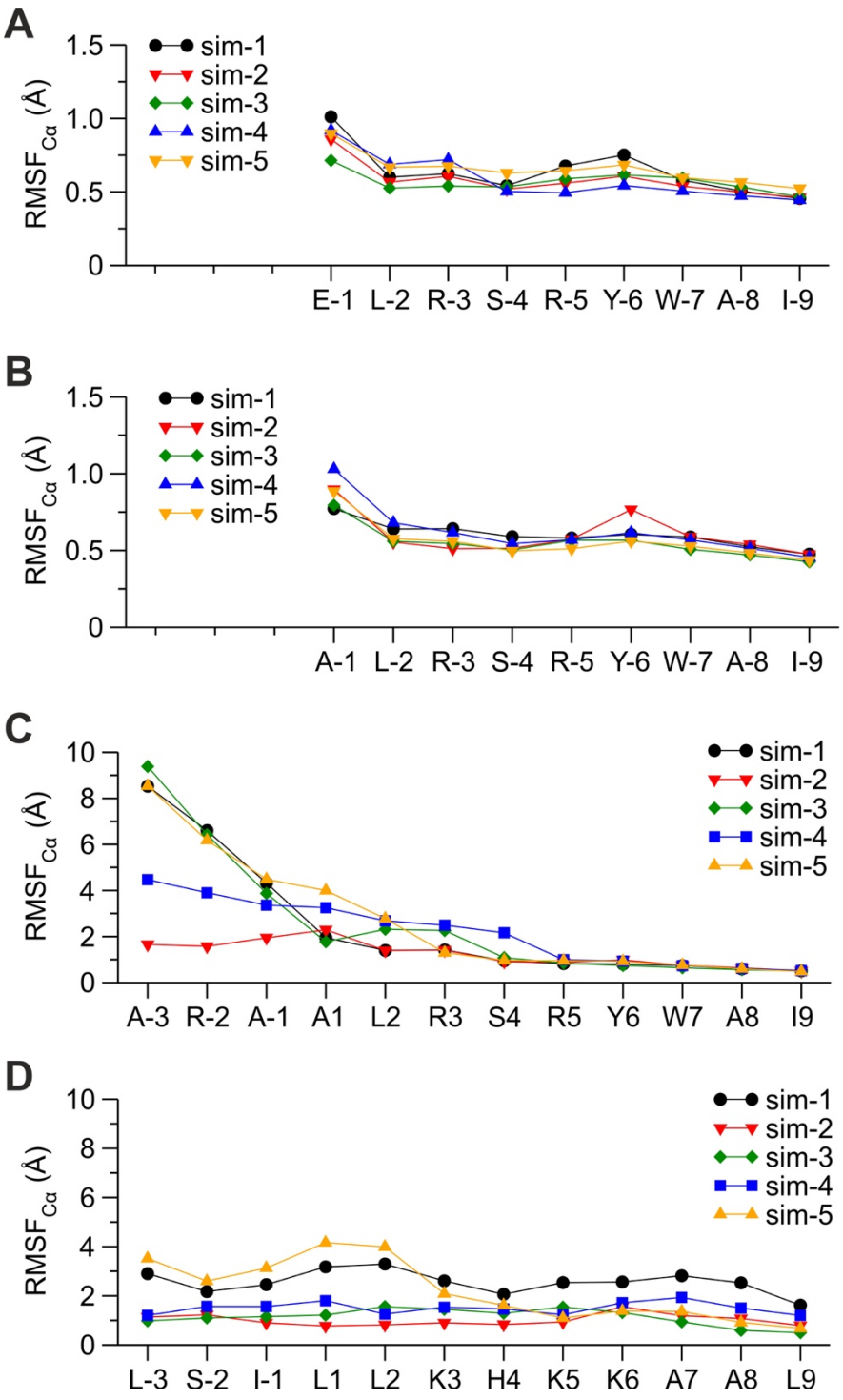

Supporting Figure 11. (A-D) Plots of the peptide C_α RMSF values extracted from each of the five MD simulations of HLA-B08 complex with the 9mer peptides EI9 (A) and AI9 (B), or the 12mer peptides AI12 (C) and LL12 (D). The corresponding plots of their mean values (± SEM) are illustrated in Figure 6.

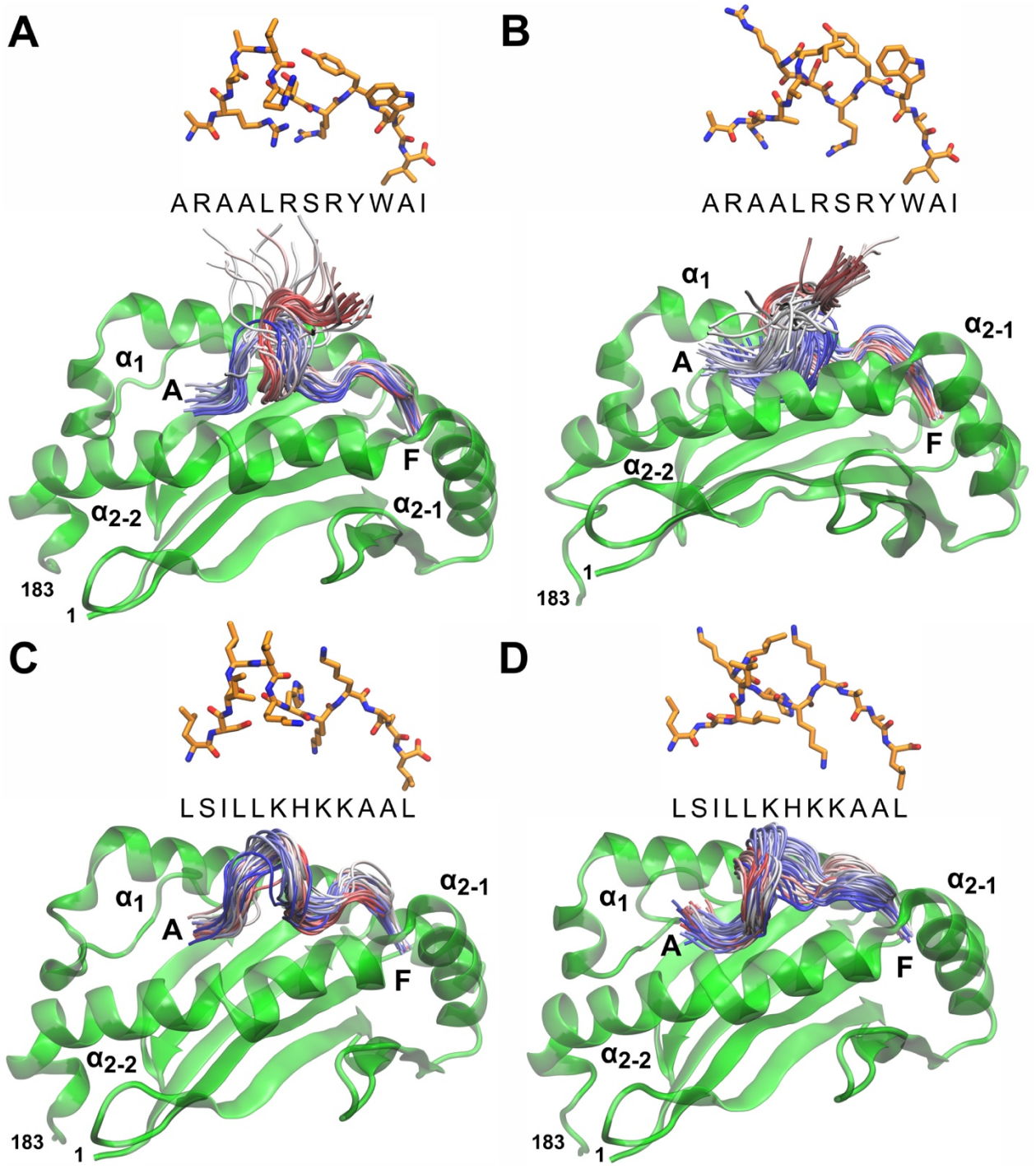

Supporting Figure 12. Ribbon representations of the HLA-B08 antigen-binding domain illustrating the backbone dynamics of the 12mer peptides from the MD simulations. Snapshots of the peptide backbone are shown as tubes and are color-coded by MD time from blue (0 ns), white (250 ns) to red (500 ns), in steps of 5 ns. The initial conformation of the peptide is shown in the same orientation of the snapshots using stick representation that is colored orange for C, blue for N and red for O atoms. (A) HLA-B08/AI12 from sim-3 (B) HLA-B08/AI12 from sim-5 (C) HLA-B08/LL12 from sim-3 (D) HLA-B08/AI12 from sim-5.

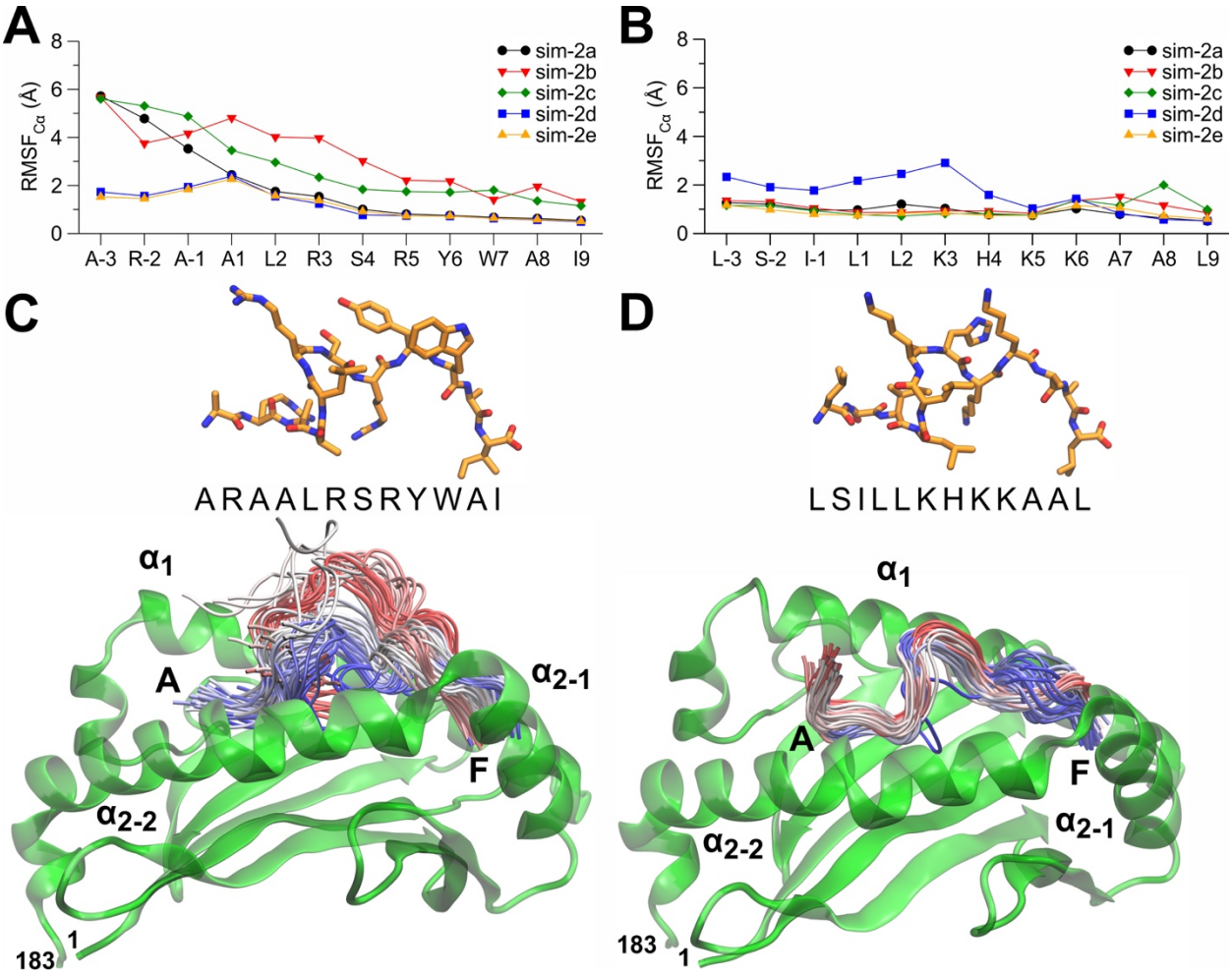

Supporting Figure 13. (A, B) Plots of the peptide C_α RMSF values extracted from five MD simulations (500 ns each) of HLA-B08 complex with the extended 12mer peptides AI12 (A) and LL12 (B), which were seeded from the initial conformation of the peptide as in sim-2 (see Supporting Figures 9, 11, 12) with different velocities. (C, D) Ribbon representations of the HLA-B08 antigen-binding domain illustrating the backbone dynamics of the 12mer peptide AI12 (C) and LL12 (D) extracted from one of the five replicate simulations (sim-2b). The peptide backbone is shown as tubes and is color-coded by MD time as in Supporting Figure 13, whereas the sticks representations on top are the initial conformations of the peptides.

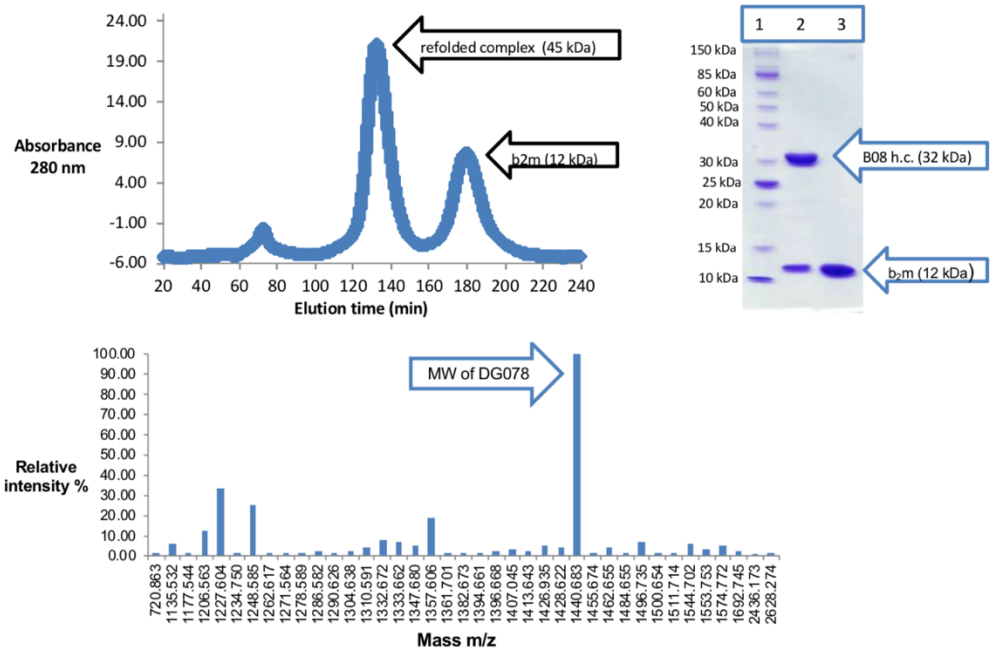

Supporting Figure 14: Folding peptide DG078 with HLA-B08. *Top left*, chromatograms depicting elution of HLA-B*08 folded in the presence of peptide DG078. *Top right*, SDS-PAGE analysis of the two major peaks of chromatogram. *Bottom*, MALDI-MS analysis of folded complex, indicating the mass of the bound peptide.

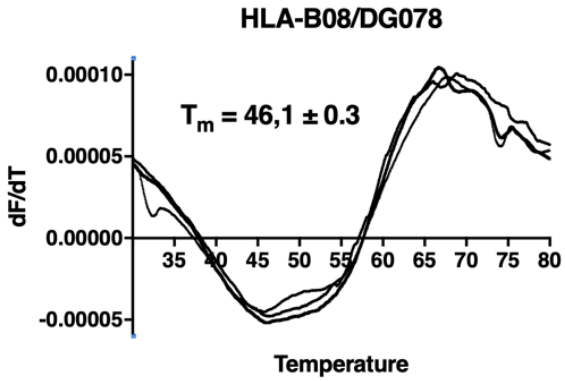

Supporting Figure 15: First derivatives of melting curves of HLA-B08 in complex with DG078 followed by Differential Scanning Fluorimetry Assay**.**

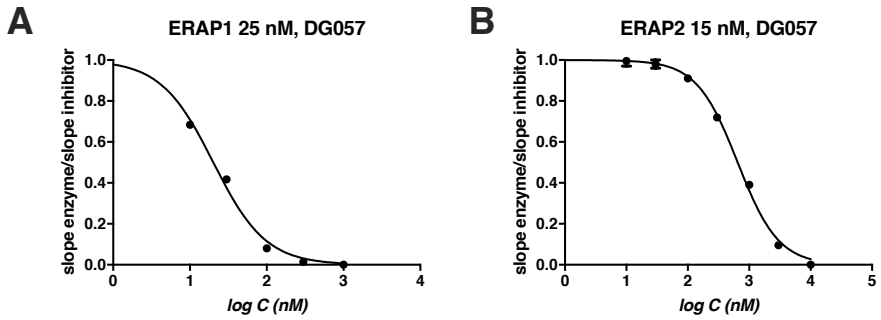

Supporting Figure 16: Effect of adding peptide DG057 on the activity of ERAP1 (panel A) or ERAP2 (panel B). Data were fit to a log (inhibitor) vs. response-variable slope model to calculate IC_{50} values.

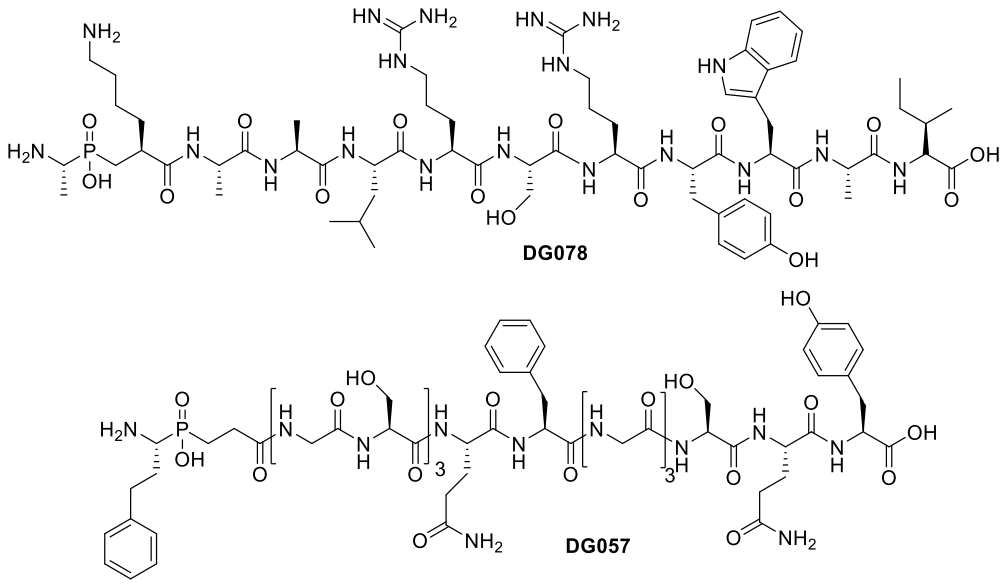

Supporting Figure 17: Structures of peptides DG057 and DG078

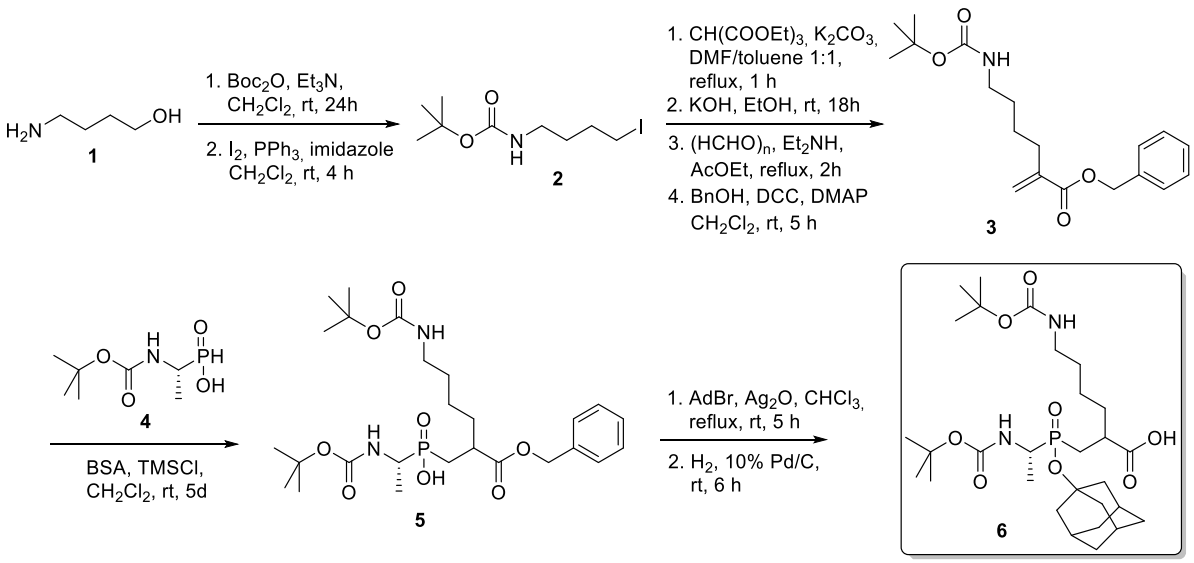

Supporting Figure 18: Synthetic route for building block Boc-(*R*)-Ala[PO(OAd)-CH_2]-(*R*,*S*)-Lys(Boc)OH